SCIENCE CHINA PRESS

SCIENCE CHINA Life Sciences
life.scichina.com link.springer.com
https://doi.org/10.1007/s11427-023-2471-4

RESEARCH PAPER

M6PR interacts with the HA2 subunit of influenza A virus to facilitate the fusion of viral and endosomal membranes

Yuzhen Hu†, Li Jiang†, Guangwen Wang, Yangming Song, Zhibo Shan, Xuyuan Wang, Guohua Deng, Jianzhong Shi, Guobin Tian, Xianying Zeng, Liling Liu, Hualan Chen* & Chengjun Li*

State Key Laboratory for Animal Disease Control and Prevention, Harbin Veterinary Research Institute, Chinese Academy of Agricultural Sciences, Harbin 150069, China

†Contributed equally to this work
*Corresponding authors (Chengjun Li, email: lichengjun@caas.cn; Hualan Chen, email: chenhualan@caas.cn)

Received 4 September 2023; Accepted 18 October 2023; Published online 22 November 2023

Influenza A virus (IAV) commandeers numerous host cellular factors for successful replication. However, very few host factors have been revealed to be involved in the fusion of viral envelope and late endosomal membranes. In this study, we identified cation-dependent mannose-6-phosphate receptor (M6PR) as a crucial host factor for the replication of IAV. We found that siRNA knockdown of M6PR expression significantly reduced the growth titers of different subtypes of IAV, and that the inhibitory effect of M6PR siRNA treatment on IAV growth was overcome by the complement of exogenously expressed M6PR. When A549 cells were treated with siRNA targeting M6PR, the nuclear accumulation of viral nucleoprotein (NP) was dramatically inhibited at early timepoints post-infection, indicating that M6PR engages in the early stage of the IAV replication cycle. By investigating the role of M6PR in the individual entry and post-entry steps of IAV replication, we found that the downregulation of M6PR expression had no effect on attachment, internalization, early endosome trafficking, or late endosome acidification. However, we found that M6PR expression was critical for the fusion of viral envelope and late endosomal membranes. Of note, M6PR interacted with the hemagglutinin (HA) protein of IAV, and further studies showed that the lumenal domain of M6PR and the ectodomain of HA2 mediated the interaction and directly promoted the fusion of the viral and late endosomal membranes, thereby facilitating IAV replication. Together, our findings highlight the importance of the M6PR–HA interaction in the fusion of viral and late endosomal membranes during IAV replication.

influenza A virus | M6PR | HA | membrane fusion | late endosome

INTRODUCTION

Influenza A virus (IAV) is an enveloped, segmented, negative-stranded RNA virus, belonging to *Orthomyxoviridae* family. The eight viral RNA segments encode 10 essential proteins as well as a few accessory proteins (Muramoto et al., 2013; Wise et al., 2009; Wise et al., 2012; Yamayoshi et al., 2016). On the basis of the antigenicity of the two surface glycoproteins, hemagglutinin (HA) and neuraminidase (NA), IAV is further classified into different subtypes. To date, 18 HA subtypes and 11 NA subtypes of IAV have been identified (Tong et al., 2013). IAV causes seasonal epidemics and occasional pandemics in humans. Since the beginning of the last century, there have been four human influenza pandemics: the 1918 H1N1 pandemic, 1957 H2N2 pandemic, 1968 H3N2 pandemic, and 2009 swine-origin H1N1 pandemic (Kasowski et al., 2011). In addition to these pandemics, seasonal influenza epidemics occur annually and kill an estimated 290,000–650,000 people each year (Iuliano et al., 2018). Moreover, the avian and swine influenza viruses severely threat the global animal husbandry and also occasionally infect humans, causing mild-to-severe disease and even death (Cui et al., 2022a; Cui et al., 2022b; Gao et al., 2013; Gu et al., 2022; Lai et al., 2016; Lee et al., 2021; Li and Chen, 2021; Liu et al., 2022; Meng et al., 2023; Shi et al., 2017; Shi et al., 2018).

IAV infection is initiated by HA binding to sialic acid (SA) receptors on cell surface glycoproteins or glycolipids (Rogers et al., 1983). After binding to these receptors, IAV is internalized by receptor-mediated endocytosis, including clathrin-dependent or clathrin-independent endocytosis or macropinocytosis (de Vries et al., 2011; Rust et al., 2004; Sieczkarski and Whittaker, 2002). Internalized viruses are transported from early endosomes to late endosomes, where the low pH environment triggers large conformational rearrangements in HA that expose the fusion peptide of HA2 to facilitate the fusion of viral envelope and endosomal membranes, thereby providing a pathway for the viral ribonucleoprotein (vRNP) to enter the cytoplasm (Bullough et al., 1994; Lakadamyali et al., 2003; Skehel and Wiley, 2000). To date, several host cellular factors have been shown to be involved in attachment or internalization during IAV entry through association with HA. Among them, HSP90AA1 (heat shock protein 90AA1) interacts with HA to increase IAV attachment on the surface of infected cells (Wang et al., 2020b). FFAR2 (free fatty acid receptor 2), IGDCC4 (transmembrane protein immunoglobulin superfamily DCC subclass member 4), and nucleolin interact with HA and promote the internalization of IAV into host cells (Chan et al., 2016; Song et al., 2021; Wang et al., 2020a). Regarding the fusion process of viral envelope and late endosomal membranes, it is a rate-limiting step at the post-entry stage of virus replication cycle. Therefore, a large number of studies have been carried out in this

critical research area. However, a gap remains unresolved regarding whether any host factor engages in the fusion of viral envelope and late endosomal membranes through association with HA—the central player in driving the membrane fusion of IAV.

By using genome-wide siRNA library screening, our laboratory identified a number of potential host cellular proteins involved in the replication cycle of IAV, including FFAR2 and BinCARD1, whose roles in the replication of IAV have been elucidated (Wang et al., 2020a; Wang et al., 2022b). In this study, we focused on cation-dependent mannose-6-phosphate receptor (CD-MPR, also called M6PR), which was required for IAV replication in our preliminary screen. M6PR is a 46-kD type I transmembrane glycoprotein that is found in the *trans*-Golgi-network (TGN), endosomes, and plasma membrane, but not lysosomes (Ghosh et al., 2003; Klumperman et al., 1993). M6PR belongs to the P-type lectin family, which consists of two members, M6PR and the insulin-like growth factor II/cation-independent mannose 6-phosphate receptor (IGF-II/CI-MPR). These two MPRs play an important role in delivering newly synthesized lysosomal enzymes bearing the M6P signal from the TGN to late endosomes. After the cargo enzymes are unloaded in the late endosomes, the MPRs are recycled back to the TGN to repeat this process (Bonifacino and Rojas, 2006; Pfeffer, 2009). M6PR was previously revealed to be important for the cell entry of rotaviruses and enterovirus 71 (Díaz-Salinas et al., 2014; Ohka et al., 2022), and for the transport of varicella-zoster virus (VZV) along the egress pathway from the late endosomes to the plasma membrane (Girsch et al., 2020). However, a role for M6PR in IAV infection has never been reported.

In the present study, we demonstrate that M6PR is a novel host factor with a positive regulatory effect on IAV replication. We find that M6PR plays an important role in mediating the membrane fusion process of IAV with late endosomes. Strikingly, the lumenal domain of M6PR interacts with the ectodomain of HA2, and this interaction directly promotes the fusion of the viral and late endosomal membranes, thereby facilitating the replication of IAV. This finding shows that in addition to the acidic environment of late endosomes, IAV also requires the participation of interacting host factors when membrane fusion occurs, which may provide new targets for the development of antiviral drugs.

RESULTS

M6PR is required for the replication of different subtypes of IAV

M6PR was revealed as a potential host factor required for IAV replication in a genome-wide siRNA screen by using a Venus-expressing replication-competent H5N1 virus (Wang et al., 2018). To verify this finding, the impact of siRNA-mediated M6PR knockdown on the replication of multiple IAV strains was determined. First, we analyzed the knockdown efficiency of M6PR-specific siRNA (siM6PR) by using quantitative reverse-transcription PCR (RT-qPCR) and Western blotting. We found that M6PR expression was reduced at both the mRNA and protein levels in siM6PR-treated A549 cells compared with scrambled siRNA-treated cells (Figure 1A and B), and that M6PR knockdown had no adverse effect on cell viability (Figure 1C). Next, we infected siRNA-treated A549 cells with a range of IAV strains: A/Anhui/2/2005 (AH05, H5N1), A/WSN/1933 (WSN, H1N1), and A/chicken/Shanghai/SC197/2013 (SH13, H9N2) (Figure 1D–F). The growth titers of all three viral strains in the siM6PR-treated A549 cells were significantly decreased at 24 and 48 h post-infection (p.i.) compared with those of scrambled siRNA-treated cells, demonstrating that M6PR is important for the efficient growth of different subtypes of IAV. To exclude the possibility of off-target siRNA effects, we repeated this experiment using another two different siRNAs targeting M6PR (siM6PR-2 and siM6PR-3). Both siRNAs substantially reduced M6PR expression (Figure 1G), and depletion of M6PR with either siRNA greatly reduced the growth titers of WSN (H1N1) virus compared with cells transfected with scrambled siRNA (Figure 1H). These results indicate that knockdown of cellular M6PR expression has an inhibitory effect on the replication of IAV.

To validate and extend these findings, we complemented the expression of M6PR in siM6PR-treated HEK293 cells by transfecting a plasmid encoding M6PR, followed by assessment of its effect on the growth property of IAV. As shown in Figure 1I, the complement of M6PR expression restored the growth titers of WSN (H1N1) virus at 24 and 48 h p.i., demonstrating that the inhibitory effect of siRNA-mediated M6PR knockdown on IAV replication is caused by the depletion of M6PR expression.

We also established an M6PR knockout (M6PR_KO) A549 cell line by using the CRISPR/Cas9 gene-editing tool. By co-electrotransfection of two pSpCas9(BB)-2A-GFP (pX458) constructs bearing single guide RNA (sgRNA) targeting M6PR into A549 cells, the M6PR_KO A549 cell clone was successfully generated, and confirmed by Western blotting with a rabbit anti-M6PR antibody (Figure 1J). M6PR knockout had no detectable effect on cell viability (Figure 1K). The titers of WSN (H1N1) virus grown in M6PR_KO A549 cells were dramatically reduced compared with those of the control cells at 24 and 48 h p.i. (Figure 1L). These results confirm that M6PR is a proviral host cellular factor for IAV replication.

M6PR is required for the early stage of the IAV replication cycle

To investigate which stage of the IAV replication cycle is affected by M6PR, A549 cells treated with siM6PR or scrambled siRNA were infected with WSN (H1N1) virus at an MOI (multiplicity of infection) of 5. At 6 and 9 h p.i., the level of viral nucleoprotein (NP) was determined by Western blotting. We found that knockdown of M6PR dramatically reduced the level of viral NP protein (Figure 2A). We also measured the vRNA, mRNA, and cRNA levels of the viral NP gene in WSN (H1N1)-infected A549 cells at 3 and 6 h p.i. by using RT-qPCR (Figure 2B). The levels of each species of viral RNA in siM6PR-treated A549 cells were significantly reduced compared with those in scrambled siRNA-treated cells, which were initially observed at 3 h p.i., indicating that M6PR most likely functions in the early stage of IAV replication. To validate this finding, we determined the cellular distribution of NP at early timepoints of infection in siRNA-treated A549 cells. The siRNA-treated cells were infected with WSN (H1N1) virus (MOI: 5), and at the indicated timepoints p.i., viral NP was stained with a mouse anti-NP mAb and visualized by confocal microscopy. A clear NP signal was visualized in the nuclei of scrambled siRNA-treated A549 control cells at 3 h p.i., whereas the cells treated with siM6PR or siRNA targeting a subunit of the vacuolar ATPase (siVATPase) (serving as a

https://doi.org/10.1007/s11427-023-2471-4

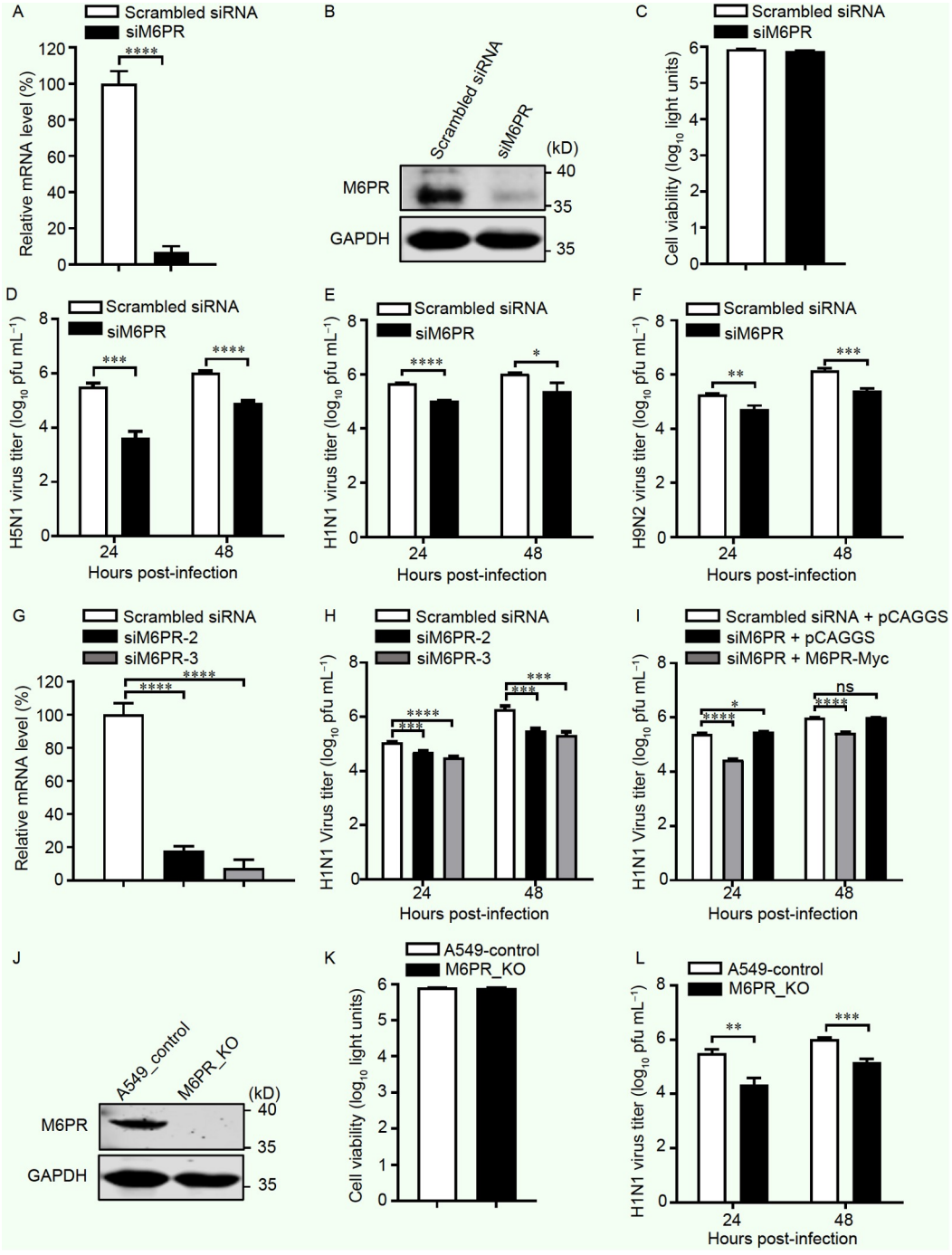

Figure 1. M6PR positively regulates IAV replication in A549 cells. A, The mRNA level of M6PR in siM6PR- or scrambled siRNA-transfected A549 cells was quantified by RT-qPCR at 36 h post-transfection. ****, $P<0.0001$. B, The siRNA knockdown of M6PR expression was confirmed by Western blotting with a rabbit anti-M6PR monoclonal antibody (mAb). C, Cell viability of siM6PR-transfected A549 cells was assessed by using a CellTiter-Glo assay. D–F, siM6PR- or scrambled siRNA-transfected A549 cells were infected with AH05 (H5N1) (MOI: 0.01) (D), WSN (H1N1) (MOI: 0.01) (E), or SH13 (H9N2) virus (MOI: 0.1) (F). At the indicated timepoints p.i., supernatants were collected and titrated for infectious viruses by plaque assays on MDCK cells. *, $P<0.05$; **, $P<0.01$; ***, $P<0.001$; ****, $P<0.0001$. G, The mRNA level of M6PR in A549 cells transfected with additional siRNAs targeting M6PR was quantified by RT-qPCR at 36 h post-transfection. ****, $P<0.0001$. H, A549 cells transfected with additional siRNAs targeting M6PR were infected with WSN (H1N1) (MOI: 0.01). At the indicated timepoints p.i., supernatants were collected and titrated for infectious viruses by plaque assays on MDCK cells. ***, $P<0.001$; ****, $P<0.0001$. I, Overexpression of M6PR restores the growth of WSN (H1N1) virus in siM6PR-treated HEK293 cells. siM6PR- or scrambled siRNA-treated HEK293 cells were transfected with the indicated plasmids. At 24 h post-transfection, the cells were infected with WSN (H1N1) virus (MOI: 0.1). At the indicated timepoints p.i., supernatants were collected and titrated for infectious viruses by plaque assays on MDCK cells. *, $P<0.05$; ****, $P<0.0001$; ns, not significant. J, The knockout of M6PR in M6PR_KO A549 cells was confirmed by Western blotng with a rabbit anti-M6PR mAb. K, The viability of M6PR_KO A549 cells and A549 control cells were assessed by using the CellTiter-Glo assay. L, M6PR_KO A549 cells or A549 control cells were infected with WSN (H1N1) (MOI: 0.01). At the indicated timepoints p.i., supernatants were collected and titrated for infectious viruses by plaque assays on MDCK cells. **, $P<0.01$; ***, $P<0.001$. Data are representative of at least three independent experiments. Means±SD are shown in (A, C–I, K, L) ($n=3$).

positive control) showed a dramatic reduction in nuclear staining of NP (Figure 2C). Viral NP accumulated in the nucleus of 47% and 100% of scrambled siRNA-treated A549 cells at 2 and 3 h p.i., respectively (Figure 2D). In contrast, viral NP was only

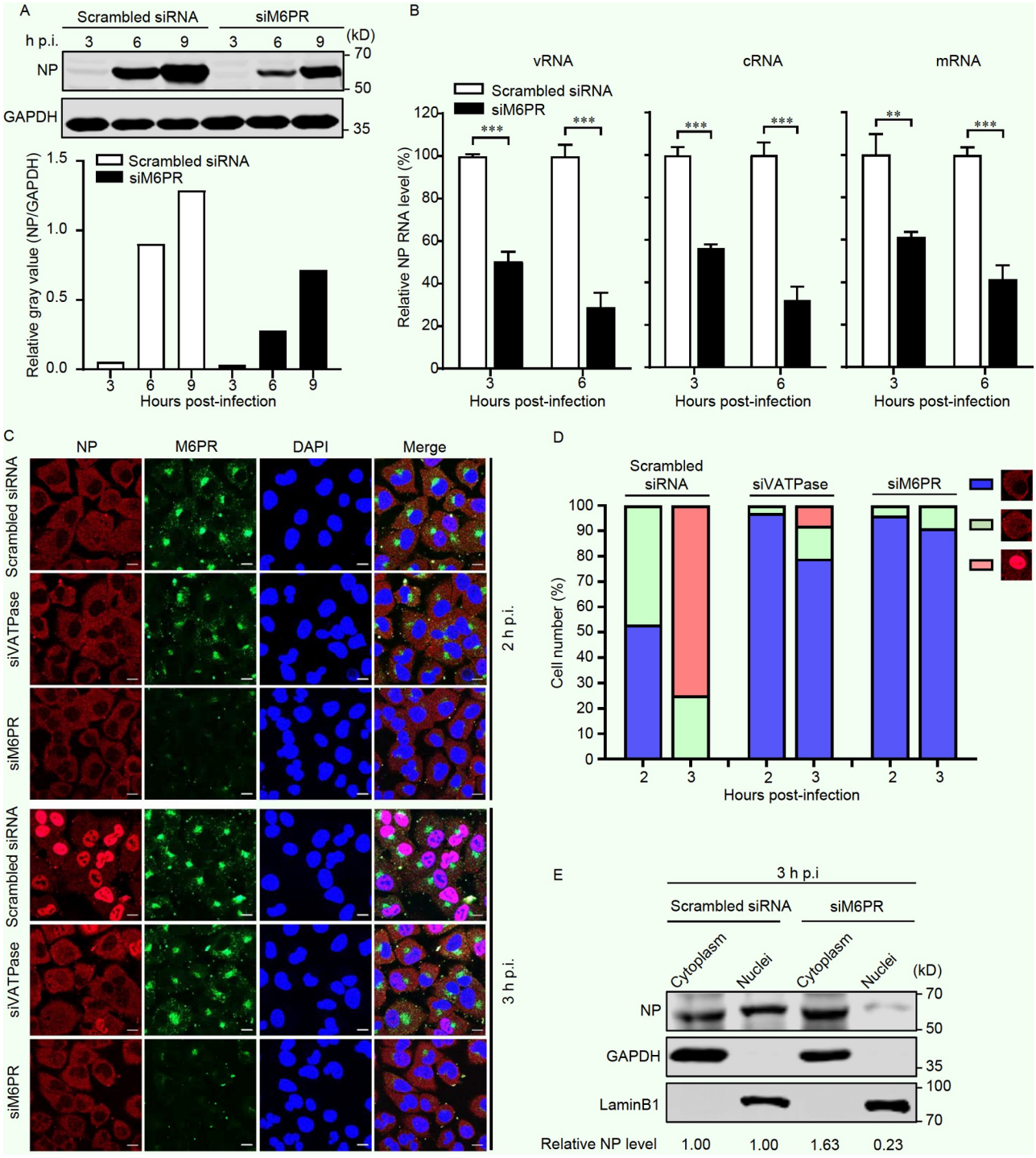

Figure 2. M6PR is required for the early stage of the IAV life cycle. A, siM6PR- or scrambled siRNA-treated A549 cells were infected with WSN (H1N1) virus (MOI: 5). Whole-cell lysates were prepared at the indicated timepoints and Western blotted with a rabbit anti-NP pAb. B, The effect of M6PR downregulation on the levels of viral RNAs. siM6PR- or scrambled siRNA-treated A549 cells were infected with WSN (H1N1) virus (MOI: 5). The levels of vRNA, mRNA, and cRNA of the NP gene were detected by RT-qPCR at 3 and 6 h p.i. **, $P<0.01$; ***, $P<0.001$. C, The effect of M6PR knockdown on the cellular distribution of NP in the early stage of the IAV replication cycle. WSN (H1N1) virus (MOI: 5) was used to infected A549 cells that were treated with siM6PR, siVATPase or scrambled siRNA for 36 h. At 2 and 3 h p.i., the infected cells were fixed and stained with a rabbit anti-M6PR mAb and a mouse anti-NP mAb, followed by incubation with Alexa Fluor 488 goat anti-rabbit IgG (H+L) (green) and Alexa Fluor 633 goat anti-mouse IgG (H+L) (red). The nuclei were stained in blue with DAPI. Scale bars, 10 μm. D, Quantitative analysis of NP localization in siRNA-treated, WSN (H1N1)-infected A549 cells. Based on the confocal microscopy images in (C), the localization of NP (indicative of vRNP) in the early stage of the virus replication cycle was categorized into three types: no nuclear localization, weak nuclear localization, and strong nuclear localization. The results shown are calculated from 100 cells visualized under a 40X objective lens. E, Cell fractionation experiment to analyze the effect of M6PR knockdown on the nuclear import of incoming vRNP complex. siM6PR- or scrambled siRNA-treated A549 cells were infected with WSN (H1N1) virus (MOI: 5) in the presence of cycloheximide (100 μg mL^{-1}). At 3 h p.i., the nuclear and cytoplasmic fractions of cells were separated and Western blotted with a rabbit anti-NP pAb, a rabbit anti-Lamin B1 pAb, and a rabbit anti-GAPDH pAb. Densitometry measurement of the Western blots was carried out with ImageJ software. Data are representative of at least two or three independent experiments. Means±SD are shown in (B) (n=3).

https://doi.org/10.1007/s11427-023-2471-4

observed in the nucleus of 4% and 9% of siM6PR-treated cells, and 3% and 21% of siVATPase-treated cells at the same timepoints (Figure 2D). These results demonstrate that M6PR downregulation impairs the early stage of the IAV replication cycle.

The inhibitory effect of M6PR downregulation on viral NP localization was confirmed in a cell fractionation experiment. We infected siM6PR- or scrambled siRNA-treated A549 cells with WSN (H1N1) virus (MOI: 5). At 3 h p.i., the lysates of infected cells were separated into cytoplasmic and nuclear fractions, and subjected to Western blotting. As shown in Figure S1 in Supporting Information, the marker proteins Lamin B1 and glyceraldehyde-3-phosphate dehydrogenase (GAPDH) were only detected in the nucleus and cytoplasm, respectively. Of note, the NP level was much lower in the nuclear extracts of the M6PR-downregulated A549 cells than in the scrambled siRNA-treated cells, indicating that M6PR knockdown disrupts the early stage of the virus replication cycle. To further determine whether M6PR plays a role in the nuclear import of the incoming vRNP complex, we also repeated this experiment in the presence of cycloheximide, a protein translation inhibitor, to block the synthesis of new NP. We found that the level of NP in the nuclei of siM6PR-treated cells was remarkably lower than that of scrambled siRNA-treated cells (Figure 2E), indicating that the nuclear import of the incoming vRNP complex is dramatically inhibited due to M6PR downregulation. These results confirm that M6PR is critical for the early stage of the virus replication cycle.

M6PR is not required for attachment, internalization, or early endosomal trafficking of IAV

To further examine the role of M6PR in the early stage of the IAV replication cycle, we assessed the impact of M6PR knockdown on the entry and early post-entry steps. First, we tested the effect of siM6PR treatment on viral attachment to the cell surface. A549 cells transfected with the siM6PR or scrambled siRNA were infected with WSN (H1N1) virus (MOI: 5) at 4°C for 1 h and then washed five times with ice-cold phosphate-buffered saline (PBS) (pH=7.2) or acidic PBS (pH=1.3), with the latter treatment being able to elute uninternalized virus particles on the cell surface (Song et al., 2021; Wang et al., 2020a; Wang et al., 2022b). The amount of virus attached on the cell surface was evaluated by assessing the amount of viral NP protein by Western blotting. As shown in Figure 3A, when washed with PBS (pH=7.2), the amount of viral NP protein on the surface of siM6PR-treated A549 cells was comparable to that of the scrambled siRNA-treated cells; however, when washed with acidic PBS (pH=1.3), the viral NP protein of cells treated with both siRNAs was nearly undetectable. These results indicate that M6PR does not exert a role in IAV attachment to the cell surface.

Next, we evaluated the effect of siM6PR treatment on IAV internalization. A second set of A549 cells pretreated as above was incubated at 37°C for 1 h after the infection at 4°C to enable the virus to get internalized. After being washed with ice-cold PBS (pH=7.2) or acidic PBS (pH=1.3), the cells were lysed and the amount of total NP from both attached and internalized viruses (PBS washed) or the amount of NP from internalized viruses (acidic PBS washed) was detected by Western blotting. We found that the amount of viral NP protein was comparable between siM6PR- and scrambled siRNA-treated A549 cells for both the PBS- and acidic PBS-washed cells (Figure 3B). We also performed this experiment in A549 cells that were pre-treated with dynasore, a specific endocytosis inhibitor. When washed with acidic PBS, the dynasore-treated A549 cells transfected with scrambled siRNA showed clearly lower level of NP compared with those non-dynasore-treated cells transfected with scrambled siRNA or siM6PR (Figure S2 in Supporting Information). These results indicate that M6PR is not involved in the internalization step of IAV.

After internalization, the IAV particles traffic through the cytoplasm via the endosomal pathway, which is separated into early endosomes and late endosomes that can be differentiated by specific molecular markers, such as the early endosome marker EEA1 (early endosomal antigen 1) (Christoforidis et al., 1999). To examine whether M6PR plays a role in early endosomal trafficking during IAV infection, A549 cells transfected with siM6PR or scrambled siRNA were incubated with WSN (H1N1) virus (MOI: 15) on ice for 1 h. After the unbound inoculum was removed by washing with ice-cold PBS, the cells were incubated at 37°C and then fixed at 30, 45 and 60 min post-temperature shift (p.t.s.). The amount of virus in the early endosomes was determined by confocal microscopy analysis to examine the colocalization of HA and EEA1, and the percentage of HA colocalizing with EEA1 was measured by using Imaris software. The colocalization between HA and EEA1 was detected throughout the visualization timepoints, and was observed similarly between siM6PR- and scrambled siRNA-treated cells (Figure 3C; Figure S3A in Supporting Information). This result indicates that M6PR does not function during the early endosomal trafficking of IAV.

M6PR is important for the membrane fusion step of IAV, but is not required for acidification of late endosomes

After trafficking through early endosomes, viral particles are transported to late endosomes, where the low pH condition triggers membrane fusion. First, we performed confocal microscopy to visualize the colocalization of HA and lysobisphosphatidic acid (LBPA), a late endosomal marker (Sun et al., 2013), to determine whether M6PR is required for IAV trafficking through late endosomes. A549 cells were transfected with siM6PR or scrambled siRNA and then infected with WSN (H1N1) virus (MOI: 15). After being incubated on ice for 1 h, the cells were cultured at 37°C, fixed at different timepoints (90, 120 and 180 min) p.t.s., and stained for HA and LBPA for visualization by confocal microscopy. The percentage of HA colocalized with LBPA was also measured by using Imaris software to quantify the amount of HA in late endosomes. As shown in Figure 4A and Figure S3B in Supporting Information, colocalization of HA and LBPA was detected up to 120 min p.t.s. in siM6PR- and scrambled siRNA-treated cells, indicating that M6PR is not required for virus trafficking from early to late endosomes. Of note, at 180 min p.i., HA was no longer colocalized with LBPA in scrambled siRNA-treated cells, but rather was diffusely distributed in the cytoplasm. In contrast, cells treated with siM6PR still displayed colocalization of HA and LBPA, with most of the HA signals being present in LBPA-marked late endosomes rather than in the cytoplasm at this timepoint. This result indicates that M6PR is important for IAV to escape from late endosomes.

Fusion of the viral and endosomal membranes is essential for the escape of virus particles from late endosomes. To examine

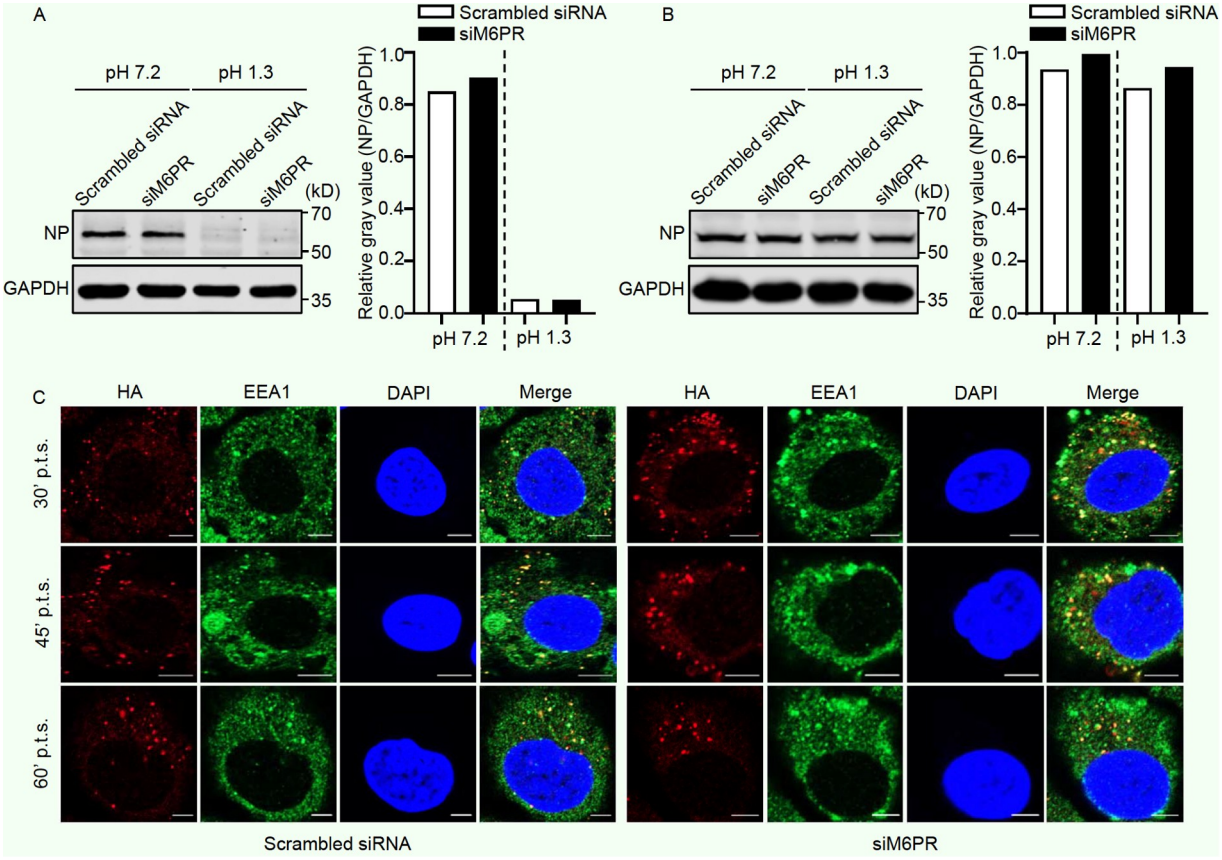

Figure 3. M6PR is not required in regulating attachment, internalization, or early endosomal trafficking of IAV. A, Western blotting to detect the amount of NP protein of WSN (H1N1) viruses attached on the surface of siM6PR- or scrambled siRNA-treated A549 cells. siM6PR- or scrambled siRNA- transfected A549 cells were incubated with WSN (H1N1) virus (MOI: 5) at 4°C for 1 h. After being washed with cold PBS (pH=7.2) or acidic PBS (pH=1.3), the amount of NP protein of viruses attached on the cell surface was detected by Western blotting with a rabbit anti-NP pAb. B, Western blotting to detect the amount of NP protein of WSN (H1N1) viruses internalized into siM6PR- or scrambled siRNA-treated A549 cells. siM6PR- or scrambled siRNA-transfected A549 cells were incubated with WSN (H1N1) virus (MOI: 5) at 4°C for 1 h, and then shifted to 37°C for 1 h. After being washed with cold PBS (pH=7.2) or acidic PBS (pH=1.3), the cells were lysed and the amount of total NP from both attached and internalized viruses (PBS washed) or the amount of NP from internalized viruses (acidic PBS washed) was detected by Western blotting with a rabbit anti-NP pAb. C, Confocal microscopy to visualize the effect of siM6PR treatment on the early endosomal trafficking of IAV. A549 cells were transfected with siM6PR or scrambled siRNA, and at 36 h post-transfection, WSN (H1N1) virus (MOI: 15) was used to infect the cells on ice for 1 h. After the inoculum was washed off with cold PBS, the culture temperature was shifted to 37°C. At the indicated timepoints post temperature shift (p.t.s.), the cells were fixed, permeabilized, and stained with a mouse anti-EEA1 mAb and a rabbit anti-HA pAb, followed by incubation with Alexa Fluor 488 goat anti-mouse IgG (H+L) (green) and Alexa Fluor 633 goat anti-rabbit IgG (H+L) (red). Scale bars, 5 μm. Data are representative of at least two or three independent experiments.

whether the depletion of M6PR inhibits membrane fusion of IAV, we generated a dual-labeled virus, which enabled us to measure membrane fusion in a quantitative manner as previously described (Wang et al., 2021). Virions labeled with two different dyes, 3,3′-dioctadecyl-5,5′-di(4-sulfophenyl) oxacarbocyanine (SP-DiOC, green) and octadecyl rhodamine B chloride (R18, red), only show red fluorescence from the R18 dye, because R18 quenches the green fluorescence from the SP-DiOC dye when they are in close proximity within the viral envelope. Once membrane fusion occurs, SP-DiOC and R18 spread into the endosomal membrane, and the green SP-DiOC signal is enhanced due to dequenching. We transfected A549 cells with siM6PR, scrambled siRNA, or siRNA targeting VATPase (a known host factor essential for endosomal acidification and viral fusion to serve as a positive control), and infected these cells with labeled viruses at 4°C for 30 min. Afterwards, the culture temperature was shifted to 37°C to enable viral entry and fusion. At 0 min p.t.s., only red fluorescence from R18 was visualized in all cells (Figure 4B). At 180 min p.t.s., both SP-DiOC and R18 were observed as speckles of green and red fluorescence in scrambled siRNA-treated cells, indicating membrane fusion had occurred. In contrast, both siM6PR- and siVATPase-treated cells displayed only few fusion sites as shown in representative images (Figure 4B). When the number of fusion sites was quantified by using the spot detection algorithm of Imaris software and normalized to the number of cell nuclei, only a few fusion sites were observed in siM6PR- and siVATPase-treated cells compared with scrambled siRNA-treated cells (Figure S3C in Supporting Information). These results demonstrate that knockdown of M6PR inhibits viral and endosomal membrane fusion.

A likely reason for the inhibition of fusion between the viral and endosomal membranes is a change in the pH of the endosome, affecting acidification. We therefore assessed the acidification of endosomes by using lysotracker (LY), a fluorescent dye that stains acidic compartments red. Before being treated with LY, siRNA-transfected A549 cells were pretreated either with dimethyl sulfoxide (DMSO) or with bafilomycin A1 (positive control), a known inhibitor of the VATPase required for endosomal acidification and viral fusion. As expected, cells treated with bafilomycin A1 displayed no lysotracker signal

https://doi.org/10.1007/s11427-023-2471-4

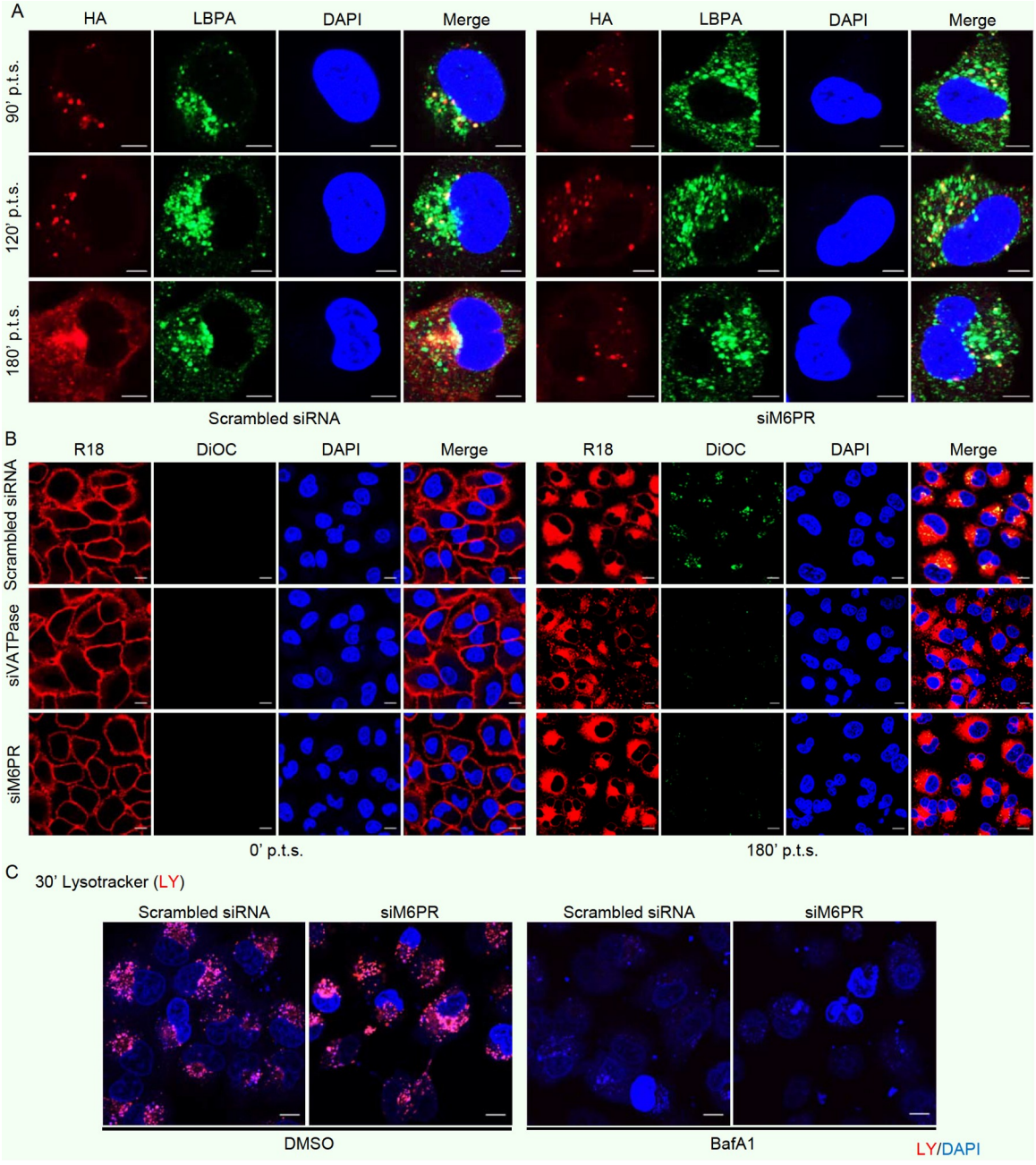

Figure 4. Knockdown of M6PR prevents fusion of viral and late endosomal membranes. A, A549 cells were transfected with siM6PR or scrambled siRNA. At 36 h post-transfection, the cells were infected with WSN (H1N1) virus (MOI: 15) on ice for 1 h. After the inoculum was washed off with cold PBS, the culture temperature was shifted to 37°C. At the indicated timepoints p.t.s., the cells were fixed, permeabilized, and stained with a mouse anti-LBPA mAb and a rabbit anti-HA pAb, followed by incubation with Alexa Fluor 488 goat anti-mouse IgG (H+L) (green) and Alexa Fluor 633 goat anti-rabbit IgG (H+L) (red). Images were acquired by confocal microscopy. Scale bars, 5 μm. B, A549 cells were transfected with the indicated siRNA, and 36 h later, the cells were infected with a dual-labeled WSN (H1N1) virus (SP-DiOC, green; R18, red) at 4°C for 30 min. The cells were then incubated at 37°C for 180 min to enable viral entry and fusion. Confocal microscopy images were acquired from cells after fixation and permeabilization. The green spots in the DiOC panel of the scrambled siRNA-treated cells indicate fusion sites. Scale bars, 10 μm. C, M6PR is not required for late endosomal acidification. A549 cells were transfected with siM6PR or scrambled siRNA. At 36 h post-transfection, the cells were treated with either DMSO or bafilomycin A1 (BafA1) for 2 h, and then labeled with lysotracker DND-99 (red) at 37°C for 30 min. Confocal microscopy images were acquired from cells without fixation or permeabilization. DAPI staining of the nucleus was achieved by adding the stain to the mounting medium. Scale bars, 10 μm. Data are representative of at least three independent experiments.

(Figure 4C, right panel). In contrast, after DMSO pretreatment, siM6PR- and scrambled siRNA-transfected cells still displayed strong lysotracker staining (Figure 4C, left panel), indicating that knockdown of M6PR does not inhibit viral fusion by altering the pH of endosomes.

Taken together, our findings indicate that M6PR is required for the fusion of the viral and late endosomal membranes, through a mechanism that does not involve the endosomal acidification event.

M6PR interacts with the HA protein of IAV

The HA protein of IAV plays a central role in mediating the fusion process of viral and late endosomal membranes. Given that

M6PR is required for the fusion of IAV with late endosomal membranes, we next explored whether M6PR interacts with HA. To this end, we performed a co-immunoprecipitation (co-IP) assay in HEK293T cells that were transfected individually or in combination with plasmids expressing V5-tagged HA of WSN (H1N1) virus and Myc-tagged M6PR. Cell lysates were immunoprecipitated with a mouse anti-V5 mAb, and then subjected to Western blotting with a rabbit anti-V5 pAb to detect WSNHA and a rabbit anti-Myc pAb to detect M6PR. We found that Myc-tagged M6PR readily co-immunoprecipitated with V5-tagged WSNHA when they were co-expressed (Figure 5A), demonstrating their interaction in mammalian cells. The specificity of the M6PR-WSNHA interaction was validated by performing a reverse co-IP experiment with a mouse anti-Myc mAb (Figure 5B). We also performed an additional co-IP experiment in HEK293T cells that were transfected with Myc-tagged M6PR and then infected with WSN (H1N1) virus (MOI: 5). At 12 h p.i., cell lysates were immunoprecipitated with a mouse anti-Myc or anti-IgG mAb, followed by Western blotting with a rabbit anti-Myc pAb for the detection of M6PR and a rabbit anti-HA pAb for the detection of HA (Figure 5C). The results showed that M6PR interacts with WSNHA during IAV infection. The physical interaction between M6PR and HA was also confirmed with three other virus strains, AH05 (H5N1), SH13 (H9N2), and FZ09 (H1N1) (Figure 5D–F), indicating that the interaction between M6PR and HA is most likely a property common to all IAV strains.

The interaction of M6PR with HA was further examined by using an immunofluorescence assay in A549 cells transfected with plasmids expressing Flag-AH05 HA and M6PR-Myc individually or in combination (Figure 5G). When expressed alone in A549 cells, HA was predominantly distributed in the plasma membrane as well as condensed areas of the cytoplasm, and M6PR was widely distributed in the cytoplasm and the plasma membrane. Notably, HA and M6PR clearly colocalized in the cytoplasm when they were co-expressed. We then determined whether HA and M6PR colocalize during IAV infection. A549 cells were infected with AH05 (H5N1) virus (MOI: 15), and at the indicated timepoints p.i., the localization of HA and M6PR was analyzed by confocal microscopy. Strikingly, we found that HA and M6PR clearly colocalized in the cytoplasm at 60 min p.i. (Figure 5H). Collectively, these findings indicate that M6PR interacts with the HA protein of IAV, which is likely the driving force to promote the membrane fusion process and overall growth of IAV.

The lumenal domain of M6PR mediates its interaction with HA and modulates the replication of IAV

Given the importance of M6PR in mediating the membrane fusion process and overall growth of IAV, we determined whether the interaction between M6PR and HA is critical for the role of M6PR in the replication of IAV. To this end, we first performed a co-IP assay to define the domain of M6PR that is important for its interaction with the HA protein of IAV. M6PR is 277 amino acids in length, containing a lumenal domain (amino acids 27–185), a transmembrane domain (amino acids 186–210), and a cytoplasmic domain (amino acids 211–277) (Figure 6A) (https://www.uniprot.org). According to the structure of M6PR, we generated two plasmids expressing either the lumenal domain or the cytoplasmic domain fused with glutathione *S*-transferase (GST) at the N-terminus (Figure 6A). By performing a GST pull-down assay in HEK293T cells transfected with the indicated combinations of plasmids, we found that the lumenal domain of M6PR is responsible for the interaction with V5-tagged WSNHA (Figure 6B).

Based on this finding, we then asked whether the interaction between M6PR and HA promotes the replication of IAV. HEK293 cells were transfected with siM6PR or scrambled siRNA. At 24 h post-transfection, the cells were further transfected with plasmids expressing GST or GST-tagged M6PR, M6PR lumenal domain, or M6PR cytoplasmic domain, respectively. Twenty-four hours later, the cells were infected with WSN (H1N1) or AH05 (H5N1) virus to assess the effect of complementing M6PR and its individual structural domains on the replication of IAV. As shown in Figure 6C and D, the complement of either M6PR or its lumenal domain in siM6PR-treated cells restored the growth titers of both WSN (H1N1) and AH05 (H5N1) virus to that of the control cells that were consecutively transfected with scrambled siRNA and GST-expressing plasmids. In contrast, the complement of the M6PR cytoplasmic domain in siM6PR-treated cells was unable to restore the virus growth titers. These results indicate that the lumenal domain of M6PR, through its interaction with the viral HA protein, is responsible for promoting the replication of IAV.

To further investigate whether the lumenal domain of M6PR facilitates IAV replication by mediating the viral fusion process, we performed the virus fusion assay. Briefly, A549 cells were first transfected with siM6PR or scrambled siRNA. At 24 h post-transfection, siRNA-treated cells were further transfected with an empty pCAGGS vector or plasmids expressing GST-tagged M6PR, M6PR lumenal domain, or M6PR cytoplasmic domain, respectively. Twenty-four hours later, the cells were infected with labeled viruses at 4°C for 30 min, and then the temperature was shifted to 37°C. As shown in Figure 6E, at 180 min p.t.s., both SP-DiOC and R18 were observed as speckles of green and red fluorescence in the scrambled siRNA-treated cells. Notably, both the SP-DiOC and R18 signals were also clearly visible in siM6PR-treated cells that were subsequently complemented with either M6PR or its lumenal domain, which was in clear contrast with cells that were consecutively transfected with siM6PR and pCAGGS vector. Furthermore, only few fusion sites were observed in siM6PR-treated cells that were complemented with the M6PR cytoplasmic domain (Figure 6E). Together, these results indicate that the lumenal domain of M6PR is responsible for the interaction with HA and for mediating the fusion of the viral and late endosomal membranes, thereby facilitating the replication of IAV.

The residues 17 to 127 of HA2 mediate the interaction with M6PR

To define the specific region in HA that binds to M6PR, we first divided HA into its two subunits, HA1 and HA2, according to its functions, and generated two constructs expressing Myc-tagged HA1 and HA2 of WSN (H1N1) virus, respectively. We then performed a GST pulldown experiment in HEK293T cells transfected with plasmids expressing GST-tagged M6PR lumenal domain, together with plasmids expressing Myc-tagged WSNHA1 or WSNHA2. We found that the HA2 subunit specifically interacted with M6PR, whereas no interaction was observed between HA1 and M6PR (Figure 7A). These results are

https://doi.org/10.1007/s11427-023-2471-4

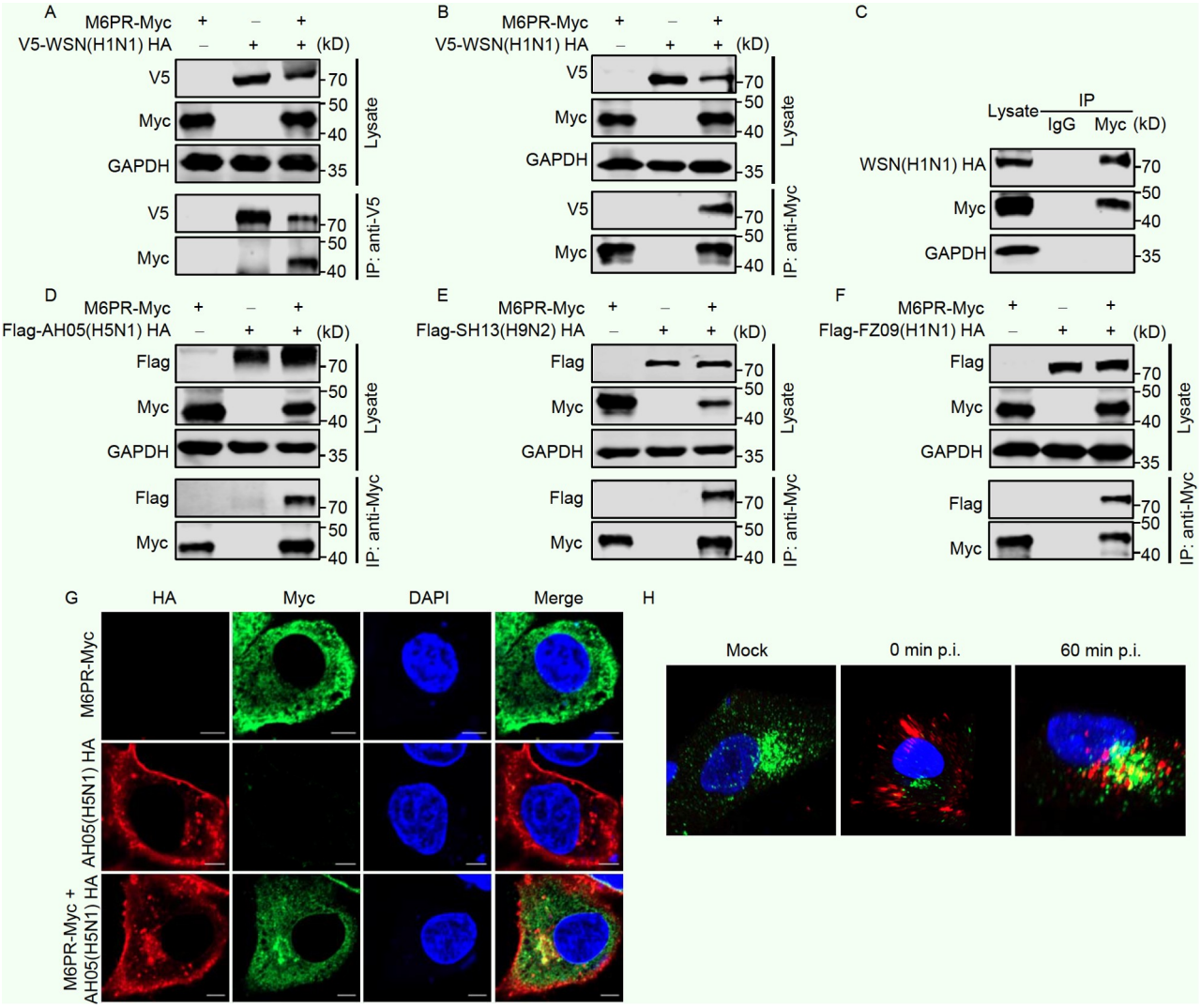

Figure 5. M6PR interacts with the HA protein of IAV. A and B, Co-IP assay to examine the interaction between M6PR and HA of WSN (H1N1) virus. HEK293T cells were transfected individually or in combination with plasmids expressing M6PR-Myc and V5-WSNHA. At 36 h post-transfection, lysates of transfected cells were immunoprecipitated with a mouse anti-V5 mAb (A) or a mouse anti-Myc mAb (B). The bound proteins were Western blotted with a rabbit anti-V5 pAb and a rabbit anti-Myc pAb to detect HA and M6PR, respectively. C, Interaction between M6PR and HA in infected cells in a Co-IP assay. HEK293T cells transfected with plasmids expressing M6PR-Myc were infected with WSN (H1N1) virus (MOI: 5) for 12 h. Lysates of infected cells were immunoprecipitated with a mouse anti-Myc mAb or anti-IgG mAb. The bound proteins were Western blotted with a rabbit anti-Myc pAb and a rabbit anti-HA pAb to detect M6PR and HA, respectively. D–F, Co-IP assay to examine the interaction between M6PR and HA of AH05 (H5N1), SH13 (H9N2), and FZ09 (H1N1) virus. HEK293T cells were transfected individually or in combination with plasmids expressing M6PR-Myc and Flag-tagged HA of AH05 (H5N1) (D), SH13 (H9N2) (E), or FZ09 (H1N1) (F). At 36 h post-transfection, cell lysates were immunoprecipitated with a mouse anti-Myc mAb. The bound proteins were Western blotted with a rabbit anti-Myc pAb and a rabbit anti-Flag pAb to detect M6PR and HA, respectively. G, Confocal microscopy analysis to visualize the colocalization of M6PR and HA in transfected A549 cells. A549 cells were transfected individually or in combination with plasmids expressing M6PR-Myc and AH05HA. At 36 h post-transfection, the cells were fixed, permeabilized, and incubated with a rabbit anti-Myc pAb and a chicken anti-HA pAb at 4°C overnight. After being stained with Alexa Fluor 633 goat anti-chicken IgG (H+L) (red) and Alexa Fluor 488 goat anti-rabbit IgG (H+L) (green), the cells were visualized by confocal microscopy. The yellow signals in the merged image indicate the colocalization of M6PR and HA. Scale bars, 5 μm. H, Confocal microscopy analysis to visualize the colocalization of M6PR and HA in virus-infected A549 cells. A549 cells were infected with AH05 (H5N1) virus (MOI: 15). At the indicated timepoints, the cells were processed as in (G), and subjected to confocal microscopy. The 3D view of colocalization was performed with Imaris software. The red, green, and yellow spots in the merged image indicate the HA, M6PR, and colocalization of M6PR and HA, respectively. Data are representative of at least two or three independent experiments.

consistent with the HA2 subunit being responsible for driving the membrane fusion process and the finding that M6PR plays a crucial role in the membrane fusion process of IAV.

Next, we attempted to narrow down the region in HA2 that is critical for interacting with M6PR. We generated six constructs expressing GST-tagged full-length HA2 (GST-HA2), cytoplasmic domain-deleted HA2 (GST-HA2delCy), cytoplasmic and transmembrane domain-deleted HA2 (GST-HA2delCy_TM), fusion peptide-deleted HA2 (GST-HA2delFP), amino acids 17–127 of HA2 (GST-$HA2_{17\text{-}127}$), and amino acids 128–185 of HA2 (GST-$HA2_{128\text{-}185}$) (Figure 7B), which were used for GST pull-down assays to examine their interaction with Flag-M6PR Lumenal. As shown in Figure 7C, the truncated mutants of HA2 lacking the N-terminal fusion peptide or the C-terminal cytoplasmic and transmembrane domains retained the ability to interact with M6PR, indicating that the main body of the HA2 ectodomain, spanning amino acids 17–185, is responsible for binding to M6PR. After generating two more truncated mutants harboring

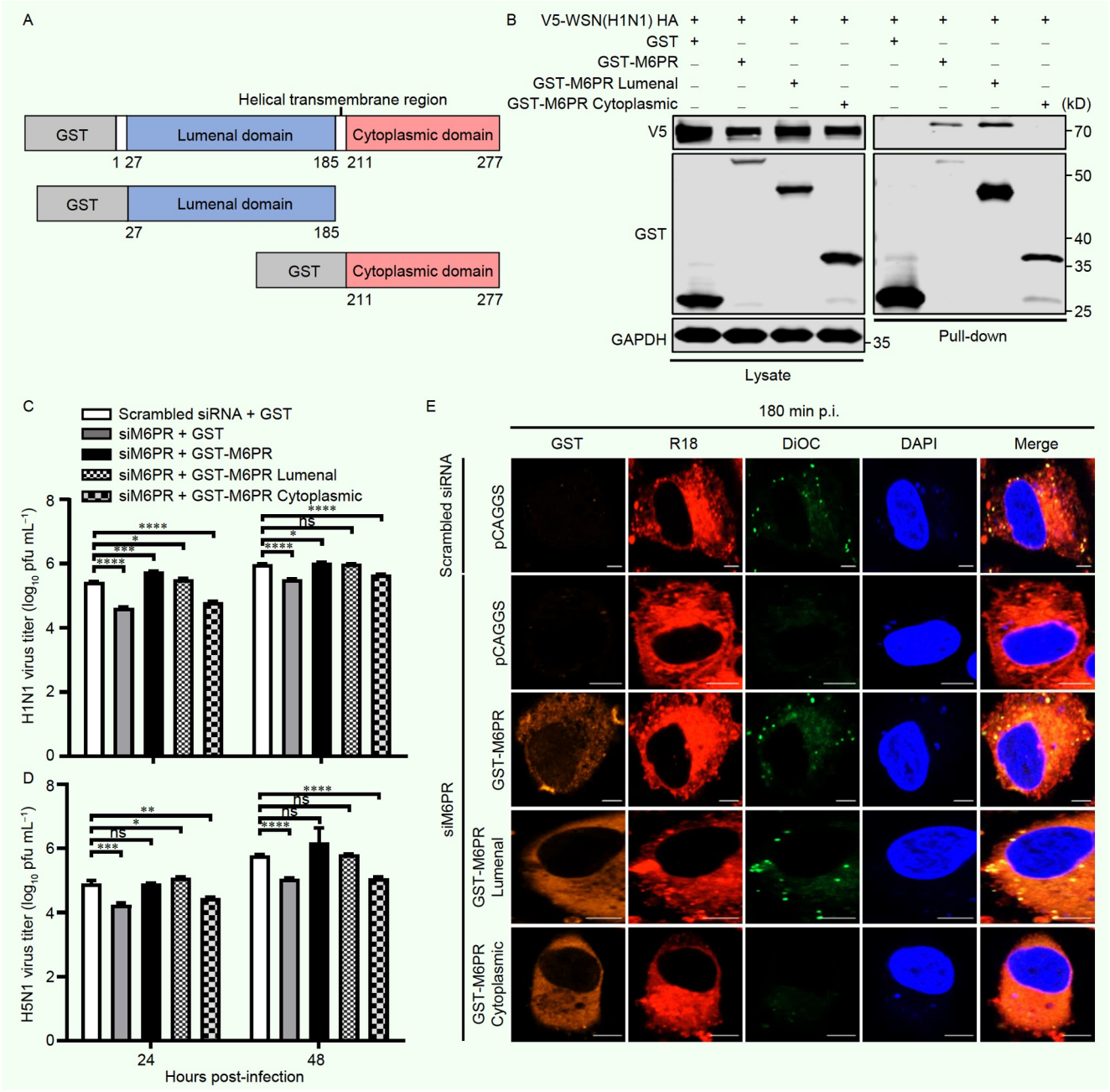

Figure 6. The lumenal domain of M6PR interacts with HA and mediates the virus fusion process. A, Schematic representation of GST-tagged M6PR and M6PR structural domains. B, GST pull-down assay to determine the specific M6PR domain that mediates the interaction with HA. HEK293T cells were transfected with plasmids expressing V5-WSNHA, together with GST, GST-M6PR, GST-M6PR Lumenal, or GST-M6PR Cytoplasmic. At 36 h post-transfection, the cell lysates were incubated with glutathione magnetic beads. The bound proteins were detected by Western blotting with a mouse anti-GST mAb and a rabbit anti-V5 pAb. C and D, Complementation of the expression of the M6PR lumenal domain in siM6PR-treated cells restores the replication of IAV. HEK293 cells were transfected with siM6PR or scrambled siRNA, and at 24 h post-transfection, the cells were further transfected with plasmids expressing GST, GST-M6PR, GST-M6PR Lumenal, or GST-M6PR Cytoplasmic. Twenty-four hours later, the cells were infected with WSN (H1N1) (C) or AH05 (H5N1) virus (D) (MOI: 0.1). At the indicated timepoints p.i., supernatants were collected and titrated for infectious viruses by plaque assays on MDCK cells. *, $P<0.05$; **, $P<0.01$; ***, $P<0.001$; ****, $P<0.0001$; ns, not significant. E, A549 cells were transfected with the indicated siRNA, and 24 h later, the cells were further transfected with the indicated plasmids. Twenty-four hours after the second transfection, the cells were infected with a dual-labeled WSN (H1N1) virus (SP-DiOC, green; R18, red) at 4°C for 30 min. The cells were then incubated at 37°C for 180 min to enable viral entry and fusion. Confocal microscopy images were acquired from cells after fixation and permeabilization. The green spots in the DiOC panel of the scrambled siRNA-treated cells indicate fusion sites. Scale bars, 5 μm. Data are representative of at least two or three independent experiments. Means±SD are shown in (C, D) (n=3).

amino acids 17–127 and 128–185 of HA2, we found that only the region spanning residues 17–127 of HA2 interacted with M6PR. These results show that the association of M6PR with the HA2 ectodomain containing the α-helix, loop, and coiled coil domains, is important for the viral fusion process.

DISCUSSION

Vaccines and antiviral drugs are the two main countermeasures used to combat IAV infection. There are currently three main classes of approved antiviral drugs against IAV: M2 ion channel

https://doi.org/10.1007/s11427-023-2471-4

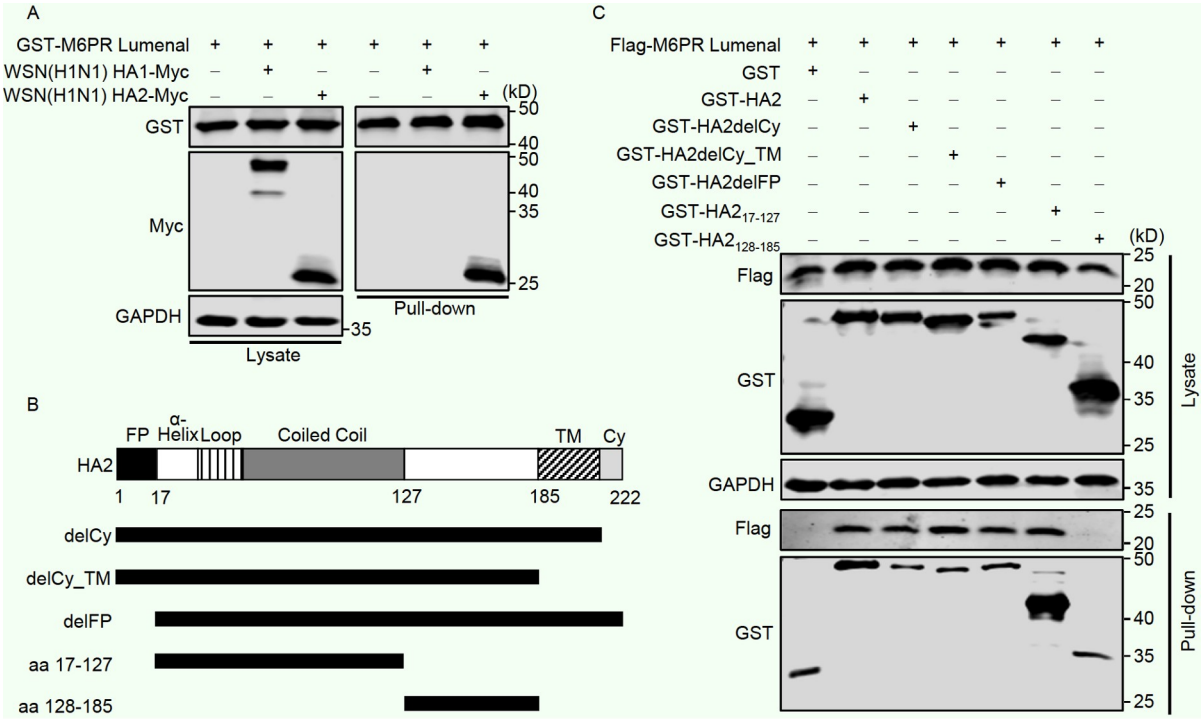

Figure 7. The residues 17 to 127 of HA2 ectodomain mediate the binding with M6PR. A, GST pull-down assay to examine the interaction of M6PR with the HA1 and HA2 subunits of IAV HA. HEK293T cells were transfected with plasmids expressing the GST-tagged M6PR lumenal domain, together with Myc-tagged HA1 or HA2 of WSN (H1N1) virus. At 36 h post-transfection, the cell lysates were incubated with glutathione magnetic beads. The bound proteins were Western blotted with a mouse anti-GST mAb and a rabbit anti-Myc pAb to detect M6PR and HA1 or HA2, respectively. B, Schematic representation of GST-tagged truncated mutants of HA2. C, GST pull-down assay to examine the interaction of M6PR with truncated mutants of HA2. HEK293T cells were transfected with plasmids expressing the Flag-tagged M6PR lumenal domain, together with GST-tagged truncated mutants of HA2 of WSN (H1N1) virus. At 36 h post-transfection, the cell lysates were incubated with glutathione magnetic beads. The bound proteins were Western blotted with a rabbit anti-Flag pAb and a mouse anti-GST mAb to detect M6PR lumenal domain and truncated mutants of HA2, respectively. Data are representative of at least two or three independent experiments.

inhibitors (amantadine and rimantadine), NA inhibitors (oseltamivir, zanamivir, and peramivir), and a PA endonuclease inhibitor (baloxavir marboxil) (O'Hanlon and Shaw, 2019). However, M2 blockers are no longer recommended for clinical use because most epidemic influenza strains have developed resistance to them, and some seasonal viruses have also developed resistance to NA inhibitors (O'Hanlon and Shaw, 2019). Moreover, drug-resistant strains have been reported following the clinical use of the PA inhibitor baloxavir marboxil (Jones et al., 2020). Given these circumstances, it is essential that we develop novel antiviral drugs that not only target viral proteins but also drugs that target viral-host interactions. Therefore, a deep understanding on the molecular mechanisms of the key host cellular proteins affecting the life cycle of IAV is essential to discover host targets for antiviral drug development. To date, many techniques have been used to identify host factors that act in the IAV life cycle, including yeast two-hybrid screens (Luo et al., 2018; Shapira et al., 2009; Wang et al., 2022a; Zhu et al., 2017), co-IP/mass spectrometry screens (Gorai et al., 2012; Watanabe et al., 2014; York et al., 2014), genome-wide siRNA screens (Brass et al., 2009; Hao et al., 2008; Karlas et al., 2010; König et al., 2010), and the newly developed CRISPR/Cas9 screens (Han et al., 2018; Song et al., 2021). The early stage of the IAV life cycle can be divided into multiple steps: attachment, internalization, early endosome trafficking, acidification, membrane fusion, and uncoating (Su et al., 2013). Given that the production of viral products has not been initiated in the early stage of the IAV life cycle, it is highly desirable to develop antiviral drugs that target the interaction between the viral and host proteins at this stage.

In the present study, we revealed M6PR as a critical host factor for the efficient replication of IAV. Knockdown or knockout of M6PR expression decreased the growth titers of different subtypes of IAV, and different siRNAs against M6PR produced the same phenotype, thereby excluding off-target effects of the siRNAs. Moreover, complement of M6PR expression in siM6PR-treated HEK293 cells reversed the inhibitory effect of M6PR knockdown on IAV replication. We further found that down-regulation of M6PR expression significantly inhibited the nuclear accumulation of NP (indicative of the nuclear import of incoming vRNP complex) at early timepoints after IAV infection in A549 cells, demonstrating that M6PR is involved in the early stage of IAV replication cycle. When dissecting the specific entry and post-entry steps of the viral replication cycle, we found that M6PR knockdown had no effect on virus attachment, internalization, or early endosomal trafficking in A549 cells. However, we discovered that upon M6PR knockdown, IAV is sequestered in late endosomes instead of escaping to the cytoplasm, indicating that the fusion of the viral envelope and late endosomal membrane was blocked.

Membrane fusion mediated by the HA protein of IAV is an essential process used by the virus to release its vRNP complex into the cytoplasm of infected cells. As a rate-limiting step in the virus replication cycle, numerous studies have investigated the membrane fusion process of IAV with late endosomes. In native viral particles, each monomer of homotrimeric HA consists of

two disulfide-bonded subunits, HA1 and HA2, responsible for receptor binding and membrane fusion (Skehel and Wiley, 2000). When IAV particles traffic to late endosomes along the endosomal pathway, the low pH environment in the late endosomes created from endosomal acidification triggers a conformational change in HA from its metastable pre-fusion conformation to a low-energy post-fusion hairpin structure (Carr et al., 1997; Carr and Kim, 1993). During this process, the N-terminal fusion peptide of HA2 that had been buried within the HA molecule is released and inserts into the endosomal membrane (Skehel et al., 1982; Stegmann et al., 1991), forming an extended intermediate conformation of HA2 (Bullough et al., 1994; Carr and Kim, 1993; Das et al., 2018). Collapse of this extended intermediate structure in the transition to post-fusion HA draws the viral and endosomal membranes together and promotes fusion (Park et al., 2003). Given the importance of the low pH environment to the fusion process of IAV, we asked whether M6PR has a role in endosomal acidification and found no detectable changes in endosomal pH when M6PR was downregulated in siM6PR-treated cells, thereby excluding the possibility that M6PR engages in the acidification of late endosomes.

Due to the central role of viral HA protein in driving the membrane fusion process of IAV, we then examined whether M6PR interacts directly with HA and, if so, whether their interaction plays a role in the membrane fusion process. By using a co-IP assay and confocal microscopy, we demonstrated that M6PR can interact with the viral HA of different subtypes of IAV. According to the structure of M6PR, we generated two truncated M6PR constructs that expressed the short C-terminal cytoplasmic domain and the N-terminal lumenal domain, respectively, and examined their interaction with HA. The GST pull-down assay revealed that only the lumenal domain of M6PR interacts with HA. Of note, complementing the M6PR lumenal domain in siM6PR-treated HEK293 cells could overcome the inhibitory effect of M6PR knockdown on IAV replication. Importantly, we found that exogenous expression of the M6PR lumenal domain in siM6PR-treated cells restored the viral fusion process to its normal state. Our findings therefore indicate that the role of M6PR in promoting the replication of IAV can be directly attributed to its ability to interact with HA and consequently facilitate the membrane fusion process of IAV with late endosomes. Although two other host proteins, Cathepsin W and CD81, also play roles in the membrane fusion process of IAV, there is no direct interplay between them and the viral HA protein, the central player of the viral fusion process. The proteolytic activity of Cathepsin W is required for the escape of IAV from late endosomes (Edinger et al., 2015), and CD81-positive endosomes are required for IAV particles to traffic to and undergo viral fusion (He et al., 2013). In contrast, M6PR is the only host cellular protein thus far known to facilitate the membrane fusion process of IAV by interacting directly with HA.

Within the HA molecule, the HA2 subunit is responsible for mediating the membrane fusion process. In our study, we revealed that M6PR specifically interacts with the HA2 subunit of HA, which is consistent with the role of M6PR in facilitating the membrane fusion process of IAV. Based on the structural characteristics of HA2 (Kim et al., 2011), we generated a set of HA2 truncation mutants and examined their interactions with M6PR. The deletion of the fusion peptide in the N-terminus of HA2 had no adverse effect on the interaction between HA2 and M6PR even though the fusion peptide is important for the membrane fusion process. In addition, deletion of the cytoplasmic and transmembrane domains in the C-terminus of HA2 did not affect the interaction with M6PR. Notably, among the HA2 truncation mutants, only the HA2 ectodomain spanning amino acids 17–127 interacted with M6PR. Previous studies have shown that the HA2 (amino acids 1–127) mutant can induce lipid mixing between liposomes and between cells, but the whole ectodomain, HA2 (amino acids 1–185), drives fusion beyond hemifusion to fusion pore opening, which means that the addition of amino acids 128–185 allows the peptide to resemble the whole HA protein more closely with regard to its ability to form a fusion pore (Epand et al., 1999; Kim et al., 2011; Leikina et al., 2001). Given that M6PR interacts with only amino acids 17–127 of HA2 ectodomain, we speculate that their interaction may contribute to the hemifusion stage. In the future, structural characterization of the M6PR-HA2 interaction during the membrane fusion process would be beneficial for designing desirable targeted antiviral drugs.

In summary, here we identified M6PR as a novel host factor for the efficient replication of IAV and demonstrated its involvement in the fusion of viral and late endosomal membranes (Figure 8). Mechanistically, the lumenal domain of M6PR interacts with the residues 17-127 of HA2 subunit of HA, which consequently facilitates the virus fusion process. Our data thus offer an in-depth insight into the post-entry stage of IAV replication cycle, which may help in the development of antiviral drugs.

MATERIALS AND METHODS

Cells and viruses

Human lung carcinoma cells (A549), human embryonic kidney cells (HEK293 and HEK293T), and Madin-Darby canine kidney (MDCK) cells were cultured in F-12K medium (Life Technologies, USA) containing 10% fetal bovine serum (FBS; Sigma-Aldrich, USA), DMEM (Life Technologies) containing 10% FBS, and DMEM containing 6% newborn calf serum (NCS; Sigma-Aldrich), respectively, at 37°C in a 5% CO_2 humidified incubator. All media were supplemented with 100 U mL^{-1} penicillin and 100 μg mL^{-1} streptomycin (Life Technologies).

A/WSN/33 (WSN, H1N1), A/Anhui/2/2005 (AH05, H5N1), and A/chicken/Shanghai/SC197/2013 (SH13, H9N2) viruses were grown in MDCK cells or 10-day-old embryonated chicken eggs as previously described (Wang et al., 2018).

All H5N1 virus experiments were carried out in the enhanced animal biosafety level 3 (ABSL3) facility in the Harbin Veterinary Research Institute (HVRI) of the Chinese Academy of Agricultural Sciences (CAAS), which is approved for such use by the China National Accreditation Service for Conformity Assessment and the Ministry of Agriculture and Rural Affairs of China.

Plasmids

The M6PR gene was amplified from total mRNAs of A549 cells by RT-PCR, and cloned into the mammalian expression vector pCAGGS that contains a Myc tag at the C-terminus. The open reading frames (ORFs) of the HA gene of AH05 (H5N1), WSN (H1N1), SH13 (H9N2), and A/Fuzhou/1/2009 (FZ09, H1N1) viruses were cloned into pCAGGS bearing a Flag tag at the N-terminus. The ORF of the HA gene of AH05 (H5N1) virus was

https://doi.org/10.1007/s11427-023-2471-4

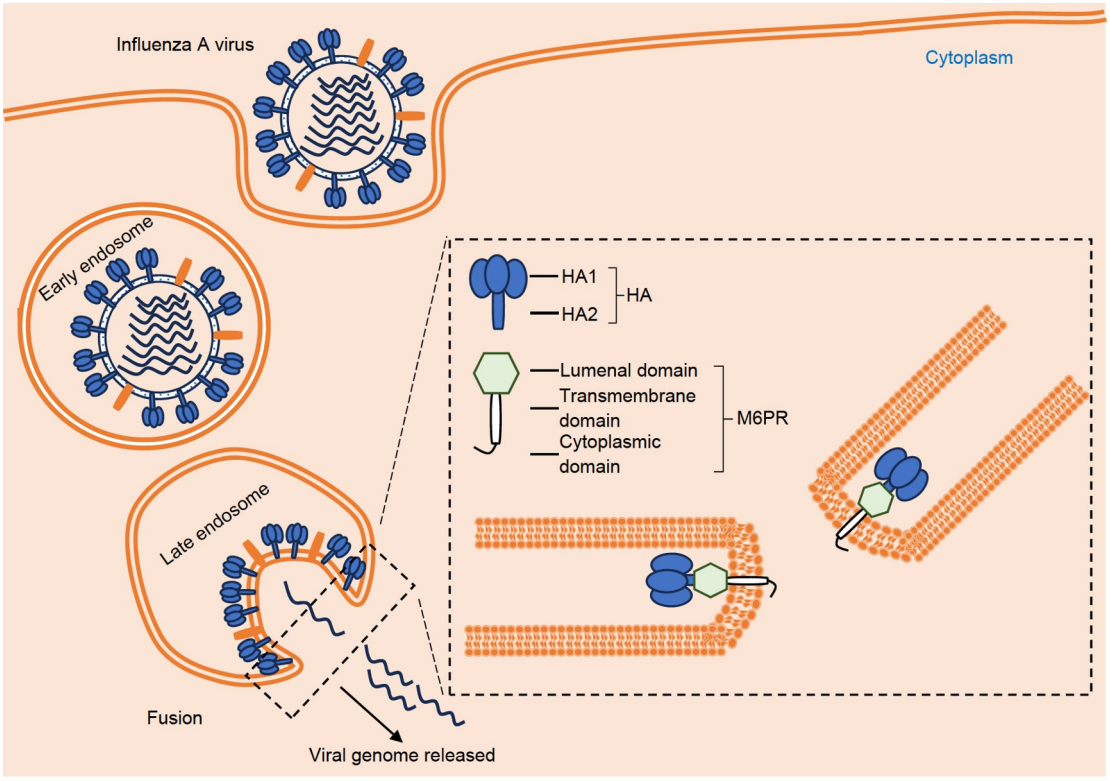

Figure 8. Schematic model showing the role of M6PR in the membrane fusion step of IAV. M6PR interacts with the HA protein of IAV, and the lumenal domain of M6PR and the ectodomain of HA2 mediate the interaction, which directly promotes the fusion of the viral and late endosomal membranes, thereby facilitating IAV replication.

also cloned into the pCAGGS vector. The pCAGGS plasmids bearing the ORFs of M6PR, M6PR-lumenal, and M6PR-cytoplasmic domain with a GST tag at the N-terminus were constructed by using a PCR approach. The coding region of M6PR-lumenal domain was also inserted into pCAGGS bearing a Flag tag at the N-terminus. The plasmids expressing full-length HA2 (GST-HA2), cytoplasmic domain-deleted HA2 (GST-HA2-delCy), cytoplasmic and transmembrane domain-deleted HA2 (GST-HA2delCy_TM), fusion peptide-deleted HA2 (GST-HA2-delFP), amino acids 17–127 of HA2 (GST-HA2$_{17\text{-}127}$), and amino acids 128–185 of HA2 (GST-HA2$_{128\text{-}185}$) were generated with a GST tag at the N-terminus by using a PCR approach. All plasmid constructs were verified by sequencing. The primer sequences used for the generation of all constructs are available upon request.

Antibodies

The following primary antibodies used in this study were obtained from commercial sources: mouse anti-Myc monoclonal antibody (mAb) (GenScript, Nanjing, China), rabbit anti-Myc polyclonal antibody (pAb) (Sigma-Aldrich), mouse anti-Flag mAb (Sigma-Aldrich), rabbit anti-Flag pAb (Sigma-Aldrich), mouse anti-GST mAb (GenScript), rabbit anti-GST pAb (Sigma-Aldrich), mouse anti-V5 mAb (GenScript), rabbit anti-V5 pAb (Sigma-Aldrich), rabbit anti-glyceraldehyde-3-phosphate dehydrogenase (GAPDH) pAb (Proteintech, Wuhan, China), rabbit anti-LaminB1 pAb (Proteintech), rabbit anti-HA pAb (Sino Biological, Beijing, China), rabbit anti-M6PR mAb (Abcam, USA), mouse anti-EEA1 mAb (BD Bioscience, USA), and mouse anti-LBPA mAb (Z-PLBPA, Echelon Bioscience, USA). The mouse anti-NP mAb, rabbit anti-NP pAb, and chicken anti-HA pAb were generated and stored in our laboratory (Zhao et al., 2022). The secondary antibodies used for confocal microscopy included Alexa Fluor 488 goat anti-rabbit IgG (H+L), Alexa Fluor 488 goat anti-mouse IgG (H+L), Alexa Fluor 633 goat anti-rabbit IgG (H+L), Alexa Fluor 633 goat anti-mouse IgG (H+L), and Alexa Fluor 633 goat anti-chicken IgG (H+L) (Life Technologies). DyLight 680 goat anti-mouse IgG (H+L), DyLight 800 goat anti-mouse IgG (H+L), and DyLight 800 goat anti-rabbit IgG (H+L), purchased from Immunoway (Plano, USA), were used as secondary antibodies for Western blotting.

siRNA sequences

The sequences of the siRNAs (Genepharma, Shanghai, China) used in this study are as follows: siM6PR (5′-GGUUCCAUCUUACUUGUCA-3′), siM6PR-2 (5′-GCUGUGGCAGUGAGAGAAU-3′), siM6PR-3 (5′-GGCUGAAACCACUGUUUAA-3′), siVATPase (5′-CGGUUAAUGAAGUCUGCUA-3′), and scrambled siRNA (5′-UUCUUCGAACGUGUCACGU-3′). All siRNAs were stored at −20°C.

siRNA transfection and virus infection

A549 cells seeded in 12-well plates were transfected with the indicated siRNA targeting M6PR or scrambled siRNA (30 nmol L^{-1}) by using the Lipofectamine RNAiMAX transfection reagent (Invitrogen, USA). The knockdown efficiency was analyzed by means of RT-qPCR and Western blotting at 36 h post-transfection. To examine the effect of M6PR knockdown on the growth of IAV, A549 cells treated with siRNA for 36 h were infected with

WSN (H1N1) or AH05 (H5N1) virus (MOI: 0.01), or SH13 (H9N2) virus (MOI: 0.1). At 24 and 48 h p.i., supernatants were collected and titrated for infectious viruses by plaque assays on MDCK cells.

In a separate experiment, HEK293 cells grown in 12-well plates were transfected with siM6PR or scrambled siRNA (30 nmol L^{-1}) by using the Lipofectamine RNAiMAX transfection reagent, and at 24 h post-transfection, the cells were further transfected with plasmids expressing GST, M6PR-GST, M6PR Lumenal-GST, or M6PR Cytoplasmic-GST. Twenty-four hours later, the cells were infected with WSN (H1N1) or AH05 (H5N1) virus (MOI: 0.1). At 24 and 48 h p.i., supernatants were collected and titrated for infectious viruses by plaque assays on MDCK cells.

Generation of M6PR_KO A549 cells and virus infection

M6PR_KO A549 cells were established by using the CRISPR/Cas9 gene-editing tool. Each of the two M6PR gene target sequences (5′-GCTACTACTACTCCTGGCTG-3′ and 5′-GAAAAAACTTGCGACTTGGT-3′) was inserted into the pSpCas9(BB)-2A-GFP (pX458) vector (Ran et al., 2013). Five micrograms of each pX458 construct bearing one of the M6PR target sequences were co-electrotransfected into A549 cells by using the Neon transfection system (Thermo Fisher Scientific, USA). Forty-eight hours later, the cells were trypsinized and sorted into single cells by using a MoFlo XDP cell sorter (Beckman Coulter, USA), and single cells were seeded into 96-well plates for colony formation. The success of generating M6PR_KO A549 cells was validated by sequencing and Western blotting. The M6PR_KO A549 cells or control cells were infected with WSN (H1N1) virus (MOI: 0.01). At 24 and 48 h p.i., supernatants were collected and titrated for infectious viruses by plaque assays on MDCK cells.

Cell viability assay

A CellTiter-Glo kit (Promega, USA) was used to assess cell viability as described previously (Luo et al., 2018; Zhu et al., 2017). In brief, cells grown in opaque-walled 96-well plates, i.e. siRNA-treated A549 cells, M6PR_KO A549 cells, or A549 control cells, were treated as in the individual experiments. Then, the cells in each well were incubated with 100 μL of CellTiter-Glo reagent for 10 min on a shaker to induce cell lysis. A GloMax 96 Microplate Luminometer (Promega) was used to measure the luminescence.

RT-qPCR

To quantify the M6PR mRNA level, an RNeasy Plus minikit (Qiagen, USA) was used to extract total RNA from siRNA-treated A549 cells at 36 h post-transfection. The synthesis of first-strand cDNA was performed with oligo(dT) primer by using the PrimeScript RT reagent kit containing gDNA Eraser (TaKaRa, Dalian, China). SYBR Premix Ex Taq II (TaKaRa) was used to conduct RT-qPCR assays with specific M6PR primers. Relative RNA quantities were examined by using the comparative cycle threshold method, in which the GAPDH gene served as the endogenous reference and scrambled siRNA-treated A549 cells served as the control.

The siRNA-treated A549 cells cultured in 12-well plates were infected with WSN (H1N1) virus (MOI: 5), followed by total RNA extraction by using the RNeasy kit at 3 and 6 h p.i. Relative quantities of genomic RNA (vRNA), complementary RNA (cRNA), and mRNA of viral NP gene were determined by RT-qPCR as described previously (Kawakami et al., 2011), using GAPDH as the endogenous reference.

Confocal microscopy

To assess the effect of M6PR knockdown on the cellular distribution of NP at early timepoints of IAV infection, WSN (H1N1) virus (MOI: 5) was used to infect A549 cells treated with siM6PR (30 nmol L^{-1}) in glass-bottom dishes. At the indicated timepoints p.i., cells were fixed with 4% PFA (paraformaldehyde) at room temperature for 30 min, treated with 0.5% Triton X-100 in PBS for 15 min, and blocked with 5% BSA in PBS for 1 h. The cells were subsequently incubated with primary antibodies (rabbit anti-M6PR mAb, 1:500; mouse anti-NP mAb, 1:500) at 4°C overnight, and then washed three times with PBS prior to incubation with the secondary antibodies (Alexa Fluor 488 goat anti-rabbit IgG (H+L), 1:500; Alexa Fluor 633 goat anti-mouse IgG (H+L), 1:500) for 1 h. After the cells were washed three times with PBS, DAPI (4′,6-diamidino-2-phenylindole; Thermo Fisher Scientific) was added to stain the nuclei for 15 min. Images were acquired with an LSM 800 confocal microscope with Airyscan (Zeiss, Germany).

In a separate experiment to observe the co-localization of M6PR and HA, A549 cells cultured in glass-bottom dishes were transfected with the indicated plasmids by using Lipofectamine LTX and Plus reagents, or were infected with AH05 (H5N1) virus (MOI: 15). At 36 h post-transfection or the indicated timepoints p.i., the cells were subjected to an immunofluorescence assay by using the indicated primary antibodies (chicken anti-HA pAb, 1:300; rabbit anti-Myc pAb, 1:500; rabbit anti-M6PR mAb, 1:500) and the corresponding secondary antibodies (Alexa Fluor 488 goat anti-rabbit IgG (H+L), 1:500; Alexa Fluor 633 goat anti-chicken IgG (H+L), 1:500), and visualized by use of confocal microscopy.

Separation of nuclear and cytoplasmic fractions

siM6PR- or scrambled siRNA-treated A549 cells cultured in 6-well plates were infected with WSN (H1N1) virus (MOI: 5). At 3 h p.i., NE-PER Nuclear and Cytoplasmic Extraction Reagents (Pierce, USA) were used to separate the cells into nuclear and cytoplasmic fractions. Western blotting was performed to detect the amount of NP, LaminB1, and GAPDH (nuclear and cytoplasmic fraction markers) in each fraction by using a rabbit anti-NP pAb, a rabbit anti-LaminB1 pAb, and a rabbit anti-GAPDH pAb, respectively.

Virus attachment and internalization assay

To examine the effect of M6PR on IAV attachment to the cell surface, we cultured A549 cells in 12-well plates and treated them with siM6PR or scrambled siRNA (30 nmol L^{-1}) for 36 h, followed by infection with WSN (H1N1) virus (MOI: 5) at 4°C for 1 h. After being washed with ice-cold PBS (pH=7.2) or acidic PBS (pH=1.3), the cells were lysed with 4× SDS-PAGE loading buffer (with β-Mercaptoethanol) (Solarbio, Beijing, China) and Western blotted with a rabbit anti-NP pAb. Acidic PBS (pH=1.3) is capable

https://doi.org/10.1007/s11427-023-2471-4

of eluting uninternalized virus particles on the cell surface (Song et al., 2021; Wang et al., 2020a; Wang et al., 2022b).

To determine the effect of M6PR on IAV internalization, we cultured A549 cells in 12-well plates and treated them with siM6PR or scrambled siRNA (30 nmol L^{-1}) for 36 h, followed by infection with WSN (H1N1) virus (MOI: 5) at 4°C for 1 h, and at 37°C for 1 h. After being washed with ice-cold PBS (pH=7.2) or acidic PBS (pH=1.3), the cells were collected and lysed for Western blotting with a rabbit anti-NP pAb.

Early and late endosomal trafficking

A549 cells treated with siM6PR or scrambled siRNA (30 nmol L^{-1}) for 36 h were infected with WSN (H1N1) virus (MOI: 15) on ice for 1 h. After washing off the inoculum with ice-cold PBS, the culture temperature was shifted to 37°C. At the indicated timepoints p.t.s., the cells were washed with PBS, fixed with 4% PFA, and treated with 0.5% Triton X-100 in PBS. The cells were then subjected to an immunofluorescence assay by using the indicated primary antibodies (mouse anti-EEA1 mAb or mouse anti-LBPA mAb, 1:300; rabbit anti-HA pAb, 1:300) and the corresponding secondary antibodies (Alexa Fluor 488 goat anti-mouse IgG (H+L), 1:500; Alexa Fluor 633 goat anti-rabbit IgG (H+L), 1:500), and visualized by use of confocal microscopy.

Virus fusion assay

Viral fusion was measured according to a protocol previously described (Sakai et al., 2006). Briefly, two fluorescent dyes, R18 (octadecyl rhodamine B chloride, 23 μmol L^{-1}) and SP-DiOC18 (3,3′-dioctadecyl-5,5′-di (4-sulfophenyl) oxacarbocyanine, 46 μmol L^{-1}) (Life Technologies), were used to label WSN (H1N1) virus. After intense vortexing at room temperature for 60 min, the labeled virus was filtered through a 0.22-μm-pore-size filter. The labeled virus was then bound to cells at 4°C for 30 min. After being washed with PBS, the cells were shifted to 37°C for 0 or 180 min, fixed with 4% PFA, treated with 0.5% Triton X-100 in PBS, and visualized by confocal microscopy.

Late endosomal acidification

A549 cells were transfected with siM6PR or scrambled siRNA (30 nmol L^{-1}). At 36 h post-transfection, the cells were treated with either DMSO or bafilomycin A1 (BafA1) for 2 h. Lysotracker red DND-99 (Life Technologies) was then diluted in F-12K medium and added to the cells (25 nmol L^{-1}). After an incubation of 30 min, the cells were washed once with PBS, and visualized by confocal microscopy without fixation or permeabilization. DAPI staining of the nuclei was achieved by adding the stain to the mounting medium.

Co-immunoprecipitation assay

The indicated plasmids were transfected into HEK293T cells cultured in 6-well plates by using the Lipofectamine LTX and Plus reagents (Invitrogen). Thirty-six hours later, the cells were lysed or infected with WSN (H1N1) virus (MOI: 5) for 12 h before the lysates were prepared. During lysate preparation, the cells were washed once with ice-cold PBS and lysed with 250 μL of IP buffer (Pierce) that contained a complete protease inhibitor cocktail (Roche Diagnostics GmbH, Germany) and PMSF (Beyotime, Shanghai, China) for 30 min on ice. After centrifugation at 13,000×*g* for 10 min at 4°C, the supernatants were immunoprecipitated with the indicated primary antibodies and rocked at 4°C overnight. Protein G-Agarose beads (Roche) were then added, and the mixture was rocked at 4°C for 6–8 h. After being washed three times with ice-cold PBS containing 1% PMSF, the immunoprecipitated proteins were separated by SDS-PAGE and detected by Western blotting.

GST pull-down assay

The indicated plasmids were transfected into HEK293T cells cultured in 6-well plates by using the Lipofectamine LTX and Plus reagents (Invitrogen). Thirty-six hours later, the cells were lysed with 250 μL of IP buffer that contained complete protease inhibitor cocktail and PMSF on ice for 30 min, and then centrifuged at 13,000×*g* for 10 min at 4°C. The supernatants were pulled down with 8 μL of glutathione magnetic agarose (Invitrogen) for 8 h, washed three times with ice-cold PBS containing 1% PMSF. The bound proteins were separated by SDS-PAGE and detected by Western blotting.

Western blotting

Protein samples separated by SDS-PAGE were transferred onto nitrocellulose membranes (GE Healthcare, USA). The membranes were blocked with 5% skim milk in PBS, and were incubated with the primary antibody diluted in Primary Antibody Dilution Buffer (Beyotime) at 4°C overnight. After incubation with DyLight 800 goat anti-mouse IgG (H+L) and DyLight 800 goat anti-rabbit IgG (H+L), an Odyssey CLX infrared imaging system (Li-Cor BioSciences, USA) was employed to visualize the blots.

Statistical analysis

Statistical analysis was performed by using the Student's two-tailed unpaired *t*-test or an analysis of variance (ANOVA) with GraphPad Prism software (GraphPad Prism 8). *P* values of<0.05 were considered significant.

Compliance and ethics

The author(s) declare that they have no conflict of interest.

Acknowledgement

This work was supported by the National Natural Science Foundation of China (32192453, 32172847), the National Key Research and Development Program of China (2021YFD1800204), the Laboratory of Lingnan Modern Agriculture Project (NT2021007), and the earmarked fund for CARS-41. We thank Susan Watson for editing the manuscript, and Dr. Yoshihiro Kawaoka (University of Wisconsin-Madison) for the gift of the pCAGGS vector.

Supporting information

The supporting information is available online at https://doi.org/10.1007/s11427-023-2471-4. The supporting materials are published as submitted, without typesetting or editing. The responsibility for scientific accuracy and content remains entirely with the authors.

References

Bonifacino, J.S., and Rojas, R. (2006). Retrograde transport from endosomes to the *trans*-Golgi network. Nat Rev Mol Cell Biol 7, 568–579.

Brass, A.L., Huang, I.C., Benita, Y., John, S.P., Krishnan, M.N., Feeley, E.M., Ryan, B. J., Weyer, J.L., van der Weyden, L., Fikrig, E., et al. (2009). The IFITM proteins mediate cellular resistance to influenza A H1N1 virus, West Nile virus, and dengue virus. Cell 139, 1243–1254.

Bullough, P.A., Hughson, F.M., Skehel, J.J., and Wiley, D.C. (1994). Structure of influenza haemagglutinin at the pH of membrane fusion. Nature 371, 37–43.

Carr, C.M., Chaudhry, C., and Kim, P.S. (1997). Influenza hemagglutinin is spring-loaded by a metastable native conformation. Proc Natl Acad Sci USA 94, 14306–

14313.
Carr, C.M., and Kim, P.S. (1993). A spring-loaded mechanism for the conformational change of influenza hemagglutinin. Cell 73, 823–832.
Chan, C.M., Chu, H., Zhang, A.J., Leung, L.H., Sze, K.H., Kao, R.Y.T., Chik, K.K.H., To, K.K.W., Chan, J.F.W., Chen, H., et al. (2016). Hemagglutinin of influenza A virus binds specifically to cell surface nucleolin and plays a role in virus internalization. Virology 494, 78–88.
Christoforidis, S., McBride, H.M., Burgoyne, R.D., and Zerial, M. (1999). The Rab5 effector EEA1 is a core component of endosome docking. Nature 397, 621–625.
Cui, P., Shi, J., Wang, C., Zhang, Y., Xing, X., Kong, H., Yan, C., Zeng, X., Liu, L., Tian, G., et al. (2022a). Global dissemination of H5N1 influenza viruses bearing the clade 2.3.4.4b HA gene and biologic analysis of the ones detected in China. Emerg Microbes Infects 11, 1693–1704.
Cui, P., Zeng, X., Li, X., Li, Y., Shi, J., Zhao, C., Qu, Z., Wang, Y., Guo, J., Gu, W., et al. (2022b). Genetic and biological characteristics of the globally circulating H5N8 avian influenza viruses and the protective efficacy offered by the poultry vaccine currently used in China. Sci China Life Sci 65, 795–808.
Das, D.K., Govindan, R., Nikić-Spiegel, I., Krammer, F., Lemke, E.A., and Munro, J.B. (2018). Direct visualization of the conformational dynamics of single influenza hemagglutinin trimers. Cell 174, 926–937.e12.
de Vries, E., Tscherne, D.M., Wienholts, M.J., Cobos-Jiménez, V., Scholte, F., García-Sastre, A., Rottier, P.J., and de Haan, C.A. (2011). Dissection of the influenza A virus endocytic routes reveals macropinocytosis as an alternative entry pathway. PLoS Pathog 7, e1001329.
Díaz-Salinas, M.A., Silva-Ayala, D., López, S., and Arias, C.F. (2014). Rotaviruses reach late endosomes and require the cation-dependent mannose-6-phosphate receptor and the activity of cathepsin proteases to enter the cell. J Virol 88, 4389–4402.
Edinger, T.O., Pohl M.O., Yángüez E., and Stertz S. (2015). Cathepsin W is required for escape of influenza A virus from late endosomes. mBio 6, e00297.
Epand, R.F., Macosko, J.C., Russell, C.J., Shin, Y.K., and Epand, R.M. (1999). The ectodomain of HA2 of influenza virus promotes rapid pH dependent membrane fusion. J Mol Biol 286, 489–503.
Gao, R., Cao, B., Hu, Y., Feng, Z., Wang, D., Hu, W., Chen, J., Jie, Z., Qiu, H., Xu, K., et al. (2013). Human infection with a novel avian-origin influenza A (H7N9) virus. N Engl J Med 368, 1888–1897.
Ghosh, P., Dahms, N.M., and Kornfeld, S. (2003). Mannose 6-phosphate receptors: new twists in the tale. Nat Rev Mol Cell Biol 4, 202–213.
Girsch, J.H., Jackson, W., Carpenter, J.E., Moninger, T.O., Jarosinski, K.W., and Grose, C. (2020). Exocytosis of progeny infectious varicella-zoster virus particles via a mannose-6-phosphate receptor pathway without xenophagy following secondary envelopment. J Virol 94, e00800-20.
Gorai, T., Goto, H., Noda, T., Watanabe, T., Kozuka-Hata, H., Oyama, M., Takano, R., Neumann, G., Watanabe, S., and Kawaoka, Y. (2012). F1Fo-ATPase, F-type proton-translocating ATPase, at the plasma membrane is critical for efficient influenza virus budding. Proc Natl Acad Sci USA 109, 4615–4620.
Gu, W., Shi, J., Cui, P., Yan, C., Zhang, Y., Wang, C., Zhang, Y., Xing, X., Zeng, X., Liu, L., et al. (2022). Novel H5N6 reassortants bearing the clade 2.3.4.4b HA gene of H5N8 virus have been detected in poultry and caused multiple human infections in China. Emerg Microbes Infects 11, 1174–1185.
Han, J., Perez, J.T., Chen, C., Li, Y., Benitez, A., Kandasamy, M., Lee, Y., Andrade, J., tenOever, B., and Manicassamy, B. (2018). Genome-wide CRISPR/Cas9 screen identifies host factors essential for influenza virus replication. Cell Rep 23, 596–607.
Hao, L., Sakurai, A., Watanabe, T., Sorensen, E., Nidom, C.A., Newton, M.A., Ahlquist, P., and Kawaoka, Y. (2008). *Drosophila* RNAi screen identifies host genes important for influenza virus replication. Nature 454, 890–893.
He, J., Sun, E., Bujny, M.V., Kim, D., Davidson, M.W., and Zhuang, X. (2013). Dual function of CD81 in influenza virus uncoating and budding. PLoS Pathog 9, e1003701.
Iuliano, A.D., Roguski, K.M., Chang, H.H., Muscatello, D.J., Palekar, R., Tempia, S., Cohen, C., Gran, J.M., Schanzer, D., Cowling, B.J., et al. (2018). Estimates of global seasonal influenza-associated respiratory mortality: a modelling study. Lancet 391, 1285–1300.
Jones, J.C., Pascua, P.N.Q., Fabrizio, T.P., Marathe, B.M., Seiler, P., Barman, S., Webby, R.J., Webster, R.G., and Govorkova, E.A. (2020). Influenza A and B viruses with reduced baloxavir susceptibility display attenuated *in vitro* fitness but retain ferret transmissibility. Proc Natl Acad Sci USA 117, 8593–8601.
Karlas, A., Machuy, N., Shin, Y., Pleissner, K.P., Artarini, A., Heuer, D., Becker, D., Khalil, H., Ogilvie, L.A., Hess, S., et al. (2010). Genome-wide RNAi screen identifies human host factors crucial for influenza virus replication. Nature 463, 818–822.
Kasowski, E.J., Garten, R.J., and Bridges, C.B. (2011). Influenza pandemic epidemiologic and virologic diversity: reminding ourselves of the possibilities. Clin Infect Dis 52, S44–S49.
Kawakami, E., Watanabe, T., Fujii, K., Goto, H., Watanabe, S., Noda, T., and Kawaoka, Y. (2011). Strand-specific real-time RT-PCR for distinguishing influenza vRNA, cRNA, and mRNA. J Virol Methods 173, 1–6.
Kim, C.S., Epand, R.F., Leikina, E., Epand, R.M., and Chernomordik, L.V. (2011). The final conformation of the complete ectodomain of the HA2 subunit of influenza hemagglutinin can by itself drive low pH-dependent fusion. J Biol Chem 286, 13226–13234.
Klumperman, J., Hille, A., Veenendaal, T., Oorschot, V., Stoorvogel, W., von Figura, K., and Geuze, H.J. (1993). Differences in the endosomal distributions of the two mannose 6-phosphate receptors. J Cell Biol 121, 997–1010.
König, R., Stertz, S., Zhou, Y., Inoue, A., Hoffmann, H.H., Bhattacharyya, S., Alamares, J.G., Tscherne, D.M., Ortigoza, M.B., Liang, Y., et al. (2010). Human host factors required for influenza virus replication. Nature 463, 813–817.
Lai, S., Qin, Y., Cowling, B.J., Ren, X., Wardrop, N.A., Gilbert, M., Tsang, T.K., Wu, P., Feng, L., Jiang, H., et al. (2016). Global epidemiology of avian influenza A H5N1 virus infection in humans, 1997–2015: a systematic review of individual case data. Lancet Infect Dis 16, e108–e118.
Lakadamyali, M., Rust, M.J., Babcock, H.P., and Zhuang, X. (2003). Visualizing infection of individual influenza viruses. Proc Natl Acad Sci USA 100, 9280–9285.
Lee, D.H., Criado, M.F., and Swayne, D.E. (2021). Pathobiological origins and evolutionary history of highly pathogenic avian influenza viruses. Cold Spring Harb Perspect Med 11, a038679.
Leikina, E., LeDuc, D.L., Macosko, J.C., Epand, R., Epand, R., Shin, Y.K., and Chernomordik, L.V. (2001). The 1−127 HA2 construct of influenza virus hemagglutinin induces cell-cell hemifusion. Biochemistry 40, 8378–8386.
Li, C., and Chen, H. (2021). H7N9 influenza virus in China. Cold Spring Harb Perspect Med 11, a038349.
Liu, K., Ding, P., Pei, Y., Gao, R., Han, W., Zheng, H., Ji, Z., Cai, M., Gu, J., Li, X., et al. (2022). Emergence of a novel reassortant avian influenza virus (H10N3) in Eastern China with high pathogenicity and respiratory droplet transmissibility to mammals. Sci China Life Sci 65, 1024–1035.
Luo, W., Zhang, J., Liang, L., Wang, G., Li, Q., Zhu, P., Zhou, Y., Li, J., Zhao, Y., Sun, N., et al. (2018). Phospholipid scramblase 1 interacts with influenza A virus NP, impairing its nuclear import and thereby suppressing virus replication. PLoS Pathog 14, e1006851.
Meng, F., Chen, Y., Song, Z., Zhong, Q., Zhang, Y., Qiao, C., Yan, C., Kong, H., Liu, L., Li, C., et al. (2023). Continued evolution of the Eurasian avian-like H1N1 swine influenza viruses in China. Sci China Life Sci 66, 269–282.
Muramoto, Y., Noda, T., Kawakami, E., Akkina, R., and Kawaoka, Y. (2013). Identification of novel influenza A virus proteins translated from PA mRNA. J Virol 87, 2455–2462.
O'Hanlon, R., and Shaw, M.L. (2019). Baloxavir marboxil: the new influenza drug on the market. Curr Opin Virol 35, 14–18.
Ohka, S., Tan, S.H., Ishiyama, E., Ogasawara, K., Hanasaka, T., Ishida, K., Hagiwara, K., Liu, C.C., Chong, P.C.S., Hanaki, K., et al. (2022). The uncoating of EV71 in mature late endosomes requires CD-M6PR. Biol Open 11, bio059469.
Park, H.E., Gruenke, J.A., and White, J.M. (2003). Leash in the groove mechanism of membrane fusion. Nat Struct Mol Biol 10, 1048–1053.
Pfeffer, S.R. (2009). Multiple routes of protein transport from endosomes to the *trans* Golgi network. FEBS Lett 583, 3811–3816.
Ran, F.A., Hsu, P.D., Wright, J., Agarwala, V., Scott, D.A., and Zhang, F. (2013). Genome engineering using the CRISPR-Cas9 system. Nat Protoc 8, 2281–2308.
Rogers, G.N., Pritchett, T.J., Lane, J.L., and Paulson, J.C. (1983). Differential sensitivity of human, avian, and equine influenza a viruses to a glycoprotein inhibitor of infection: selection of receptor specific variants. Virology 131, 394–408.
Rust, M.J., Lakadamyali, M., Zhang, F., and Zhuang, X. (2004). Assembly of endocytic machinery around individual influenza viruses during viral entry. Nat Struct Mol Biol 11, 567–573.
Sakai, T., Ohuchi, M., Imai, M., Mizuno, T., Kawasaki, K., Kuroda, K., and Yamashina, S. (2006). Dual wavelength imaging allows analysis of membrane fusion of influenza virus inside cells. J Virol 80, 2013–2018.
Shapira, S.D., Gat-Viks, I., Shum, B.O.V., Dricot, A., de Grace, M.M., Wu, L., Gupta, P. B., Hao, T., Silver, S.J., Root, D.E., et al. (2009). A physical and regulatory map of host-influenza interactions reveals pathways in H1N1 infection. Cell 139, 1255–1267.
Shi, J., Deng, G., Kong, H., Gu, C., Ma, S., Yin, X., Zeng, X., Cui, P., Chen, Y., Yang, H., et al. (2017). H7N9 virulent mutants detected in chickens in China pose an increased threat to humans. Cell Res 27, 1409–1421.
Shi, J., Deng, G., Ma, S., Zeng, X., Yin, X., Li, M., Zhang, B., Cui, P., Chen, Y., Yang, H., et al. (2018). Rapid evolution of H7N9 highly pathogenic viruses that emerged in China in 2017. Cell Host Microbe 24, 558–568.e7.
Sieczkarski, S.B., and Whittaker, G.R. (2002). Influenza virus can enter and infect cells in the absence of clathrin-mediated endocytosis. J Virol 76, 10455–10464.
Skehel, J.J., Bayley, P.M., Brown, E.B., Martin, S.R., Waterfield, M.D., White, J.M.,

Wilson, I.A., and Wiley, D.C. (1982). Changes in the conformation of influenza virus hemagglutinin at the pH optimum of virus-mediated membrane fusion. Proc Natl Acad Sci USA 79, 968–972.
Skehel, J.J., and Wiley, D.C. (2000). Receptor binding and membrane fusion in virus entry: the influenza hemagglutinin. Annu Rev Biochem 69, 531–569.
Song, Y., Huang, H., Hu, Y., Zhang, J., Li, F., Yin, X., Shi, J., Li, Y., Li, C., Zhao, D., et al. (2021). A genome-wide CRISPR/Cas9 gene knockout screen identifies immunoglobulin superfamily DCC subclass member 4 as a key host factor that promotes influenza virus endocytosis. PLoS Pathog 17, e1010141.
Stegmann, T., Delfino, J.M., Richards, F.M., and Helenius, A. (1991). The HA2 subunit of influenza hemagglutinin inserts into the target membrane prior to fusion. J Biol Chem 266, 18404–18410.
Su, W.C., Chen, Y.C., Tseng, C.H., Hsu, P.W.C., Tung, K.F., Jeng, K.S., and Lai, M.M.C. (2013). Pooled RNAi screen identifies ubiquitin ligase Itch as crucial for influenza A virus release from the endosome during virus entry. Proc Natl Acad Sci USA 110, 17516–17521.
Sun, E., He, J., and Zhuang, X. (2013). Dissecting the role of COPI complexes in influenza virus infection. J Virol 87, 2673–2685.
Tong, S., Zhu, X., Li, Y., Shi, M., Zhang, J., Bourgeois, M., Yang, H., Chen, X., Recuenco, S., Gomez, J., et al. (2013). New world bats harbor diverse influenza A viruses. PLoS Pathog 9, e1003657.
Wang, G., Jiang, L., Wang, J., Zhang, J., Kong, F., Li, Q., Yan, Y., Huang, S., Zhao, Y., Liang, L., et al. (2020a). The G protein-coupled receptor FFAR2 promotes internalization during influenza A virus entry. J Virol 94, e01707-19.
Wang, G., Zhang, J., Kong, F., Li, Q., Wang, J., Ma, S., Zhao, Y., Liang, L., Li, J., Sun, N., et al. (2018). Generation and application of replication-competent Venus-expressing H5N1, H7N9, and H9N2 influenza A viruses. Sci Bull 63, 176–186.
Wang, G., Zhao, Y., Zhou, Y., Jiang, L., Liang, L., Kong, F., Yan, Y., Wang, X., Wang, Y., Wen, X., et al. (2022a). PIAS1-mediated sumoylation of influenza A virus PB2 restricts viral replication and virulence. PLoS Pathog 18, e1010446.
Wang, X., Jiang, L., Wang, G., Shi, W., Hu, Y., Wang, B., Zeng, X., Tian, G., Deng, G., Shi, J., et al. (2022b). Influenza A virus use of BinCARD1 to facilitate the binding of viral NP to importin α7 is counteracted by TBK1-p62 axis-mediated autophagy. Cell Mol Immunol 19, 1168–1184.
Wang, X., Zheng, T., Lin, L., Zhang, Y., Peng, X., Yan, Y., Lei, J., Zhou, J., and Hu, B. (2020b). Influenza A virus induces autophagy by its hemagglutinin binding to cell surface heat shock protein 90AA1. Front Microbiol 11, 566348.
Wang, Y., Sharma, P., Jefferson, M., Zhang, W., Bone, B., Kipar, A., Bitto, D., Coombes, J.L., Pearson, T., Man, A., et al. (2021). Non-canonical autophagy functions of ATG16L1 in epithelial cells limit lethal infection by influenza A virus. EMBO J 40, e105543.
Watanabe, T., Kawakami, E., Shoemaker, J.E., Lopes, T.J.S., Matsuoka, Y., Tomita, Y., Kozuka-Hata, H., Gorai, T., Kuwahara, T., Takeda, E., et al. (2014). Influenza virus-host interactome screen as a platform for antiviral drug development. Cell Host Microbe 16, 795–805.
Wise, H.M., Foeglein, A., Sun, J., Dalton, R.M., Patel, S., Howard, W., Anderson, E.C., Barclay, W.S., and Digard, P. (2009). A complicated message: identification of a novel PB1-related protein translated from influenza A virus segment 2 mRNA. J Virol 83, 8021–8031.
Wise, H.M., Hutchinson, E.C., Jagger, B.W., Stuart, A.D., Kang, Z.H., Robb, N., Schwartzman, L.M., Kash, J.C., Fodor, E., Firth, A.E., et al. (2012). Identification of a novel splice variant form of the influenza A virus M2 ion channel with an antigenically distinct ectodomain. PLoS Pathog 8, e1002998.
Yamayoshi, S., Watanabe, M., Goto, H., and Kawaoka, Y. (2016). Identification of a novel viral protein expressed from the PB2 segment of influenza A virus. J Virol 90, 444–456.
York, A., Hutchinson, E.C., and Fodor, E. (2014). Interactome analysis of the influenza A virus transcription/replication machinery identifies protein phosphatase 6 as a cellular factor required for efficient virus replication. J Virol 88, 13284–13299.
Zhao, Y., Wen, X., Li, Q., Jiang, L., Wang, G., Liang, L., Wang, X., Chen, H., and Li, C. (2022). Generation and application of two monoclonal antibodies targeting conserved linear epitopes in the NP protein of influenza A virus. J Integr Agr 21, 2095–2105.
Zhu, P., Liang, L., Shao, X., Luo, W., Jiang, S., Zhao, Q., Sun, N., Zhao, Y., Li, J., Wang, J., et al. (2017). Host cellular protein TRAPPC6AΔ interacts with influenza A virus M2 protein and regulates viral propagation by modulating M2 trafficking. J Virol 91, e01757-16.